

Author responses to the Interactive discussion on "Fast an efficient MATLAB-based MPM solver (fMPMM-solver v1.0)" in the Geoscientific Model Development (GMD) Journal

Emmanuel Wyser, Yury Alkhimenkov, Michel Jaboyedoff, Yury Podladchikov

October 12, 2020

The referee comments appear in black, whereas our **responses** appear in blue and the **changes** made in the revised manuscript appear in red.

1 Referee #1

The paper presents an explicit vectorised form of the material point method for the generalised interpolation and CPDI2 variants of the method. The paper is reasonably written but is missing many details on the implemented algorithms and the numerical analyses are too focused on reproducing the results of others rather than on numerical performance which is the main trust of the article.

Thank you for the time spent on the revision of our work. We acknowledge the lack of details on the implemented algorithm. We developed the numerical implementation, especially the deformation framework chosen and the elasto-plastic constitutive relation. As a result, we included a subsection "3.1 Rate formulation and elasto-plasticity", which provides the reader with a detailed presentation of the constitutive relation we implemented in the solver. In addition, we focused our performance analysis for the selected case of the elasto-plastic granular collapse considering both the number of iteration per second and the number of floating-point operation per seconds with respect to the total number of material points in the system. Furthermore, we also decided to restrict our analysis to the total number of material points for two main reasons we detailed in the preamble of the Result section, as this was suggested by the second referee.

Comment # 1 The introduction to the paper appears to have picked a random selection of MPM articles rather than focusing on articles that look at the numerical implementation of the method. The introduction should be made more coherent and focused.

Reply # 1 We acknowledge the lack of coherence of the introduction section. Consequently, we focus our introduction toward the numerical implementation of MPM and add references which focus on numerical implementation of MPM and FEM, since both share common grounds. Especially, we present with greater details the concepts of vectorisation, blocking, overheads and RAM-to-cache communication issues.

Change # 1 (L31-L58) MATLAB[®] allows a rapid code prototyping but, at the expense of significantly lower computational performances than compiled language. An efficient MATLAB implementation of FEM called MILAMIN (Million a Minute) was proposed by Dabrowski et al. (2008) that was capable of solving two-dimensional linear problems with one million unknowns in one minute on a modern computer with a reasonable architecture. The efficiency of the algorithm lies on a combined use of vectorised calculations with a technique called blocking. MATLAB uses the Linear Algebra PACKages (LAPACK), written in Fortran, to perform mathematical operations by calling Basic Linear Algebra Subroutines (BLAS, Moler (2000)). The latter results in an overhead each time a BLAS call is made. Hence, mathematical operations over a large number of small matrices should be avoided and, operations on fewer and larger matrices preferred. This is

a typical bottleneck in FEM when local stiffness matrices are assembled during the integration point loop within the global stiffness matrix. Dabrowski et al. (2008) proposed an algorithm, in which a loop reordering is combined with operations on blocks of elements to address this bottleneck. However, data required for a calculation within a block should entirely reside in the CPU's cache. Otherwise, an additional time is spent on the RAM-to-cache communication and the performance decreases. Therefore, an optimal block size exists and, is solely defined by the CPU architecture. This technique of vectorisation combined with blocking significantly increases the performance.

More recently, Bird et al. (2017) extended the vectorised and blocked algorithm presented by Dabrowski et al. (2008) to the calculation of the global stiffness matrix for Discontinuous Galerkin FEM considering linear elastic problems using only native MATLAB functions. Indeed, the optimisation strategy chosen by Dabrowski et al. (2008) also relied on non-native MATLAB functions, e.g., `sparse2` of the SuiteSparse package (Davis, 2013). In particular, Bird et al. (2017) showed the importance of storing vectors in a column-major form during calculation. Mathematical operations are performed in MATLAB by calling LAPACK, written in FORTRAN, in which arrays are stored in column-major order form. Hence, element-wise multiplication of arrays in column-major form is significantly faster and thus, vectors in column-major form are recommended, whenever possible. Bird et al. (2017) concluded that vectorisation alone results in a performance increase between 13.7 and 23 times, while blocking only improved vectorisation by an additional 1.8 times. OSullivan et al. (2019) recently extended the works of Bird et al. (2017); Dabrowski et al. (2008) to optimised elasto-plastic codes for Continuous Galerkin (CG) or Discontinuous Galerkin (DG) methods. In particular, they proposed an efficient native MATLAB function, i.e., `accumarray()`, to efficiently assemble the internal force vector. Such function constructs an array by accumulation. More generally, OSullivan et al. (2019) reported a performance gain of $\times 25.7$ when using an optimised CG code instead of an equivalent non-optimised code.

Comment # 2 The authors have not picked up on any of the papers that extend the MILAMIN approach. In particular the authors should refer to the following paper that extends the MILAMIN ideas to non-linear problems: OSullivan, S, Bird, R.E., Coombs, W.M. and Giani, S. (2019). Rapid non-linear finite element analysis of continuous and discontinuous Galerkin methods in MATLAB. *Computers and Mathematics with Applications* 78(9): 3007-3026. There are others and the authors should review the appropriate literature.

Reply # 2 Indeed, we were not aware of further extension to the MILAMIN approach. We reviewed the reference proposed and found common approach concerning vectorization, i.e., the use of the `accumarray` function to accumulate internal force contributions to nodes. Additionally, we reviewed the appropriate literature and consequently update the introduction section. As such, our reply follows the previous statement of our first reply.

Change # 2 See Change # 1.

Comment # 3 If performance is the focus, why use MATLAB? Why not adopt one of the existing MPM codes that are written in compiled code which will always be faster than MATLAB? Such as: [jixiefx.com](https://github.com/jixiefx), github.com/yuanminghu/taichi_mpm, [cimne.com/kratos/](https://github.com/cimne/kratos/), github.com/nairnj/nairn-mpm-fea, github.com/cbgeo/mpm/, sourceforge.net/p/mpmgimp, github.com/xzhang66/MPM3D-F90. There may be others.

Reply # 3 It is true that MPM codes written in compiled codes will always be faster than MATLAB. Our point is to show that one can use MATLAB to produce prototyped code with a decent computational performance. However, our true concern is to propose an efficient and vectorised code, which could be more easily translated into the C/CUDA language, or, at least, which partially minimizes the hurdles of the syntax translation while preserving the algorithm. As such, we clearly state such concern in the revised manuscript.

Change # 3 (L68-70) The vectorisation of MATLAB functions is also crucial for a straight transpose of the solver to a more efficient language, such as the C-CUDA language, which allows the parallel execution of computational kernels of graphics processing units (GPUs).

(L558-560) The vectorisation activities we performed provide a fast and efficient MATLAB-based MPM solver. Such vectorised code could be transposed to a more efficient language, such as the C-CUDA language, that is known to efficiently take advantage of vectorised operations.

Comment # 4 The authors mention an implicit implementation but do not present any results in terms of the speed gains of the implicit vectorised algorithm. These should be included and the vectorised algorithm explained.

Reply # 4 It is true that i) we do not present any results related to speed gain and, ii) the implicit implementation is not explained. Our concern was to show that the error saturation we reported for the explicit implementation was due to the explicit formulation. Consequently, an implicit implementation under the vectorisation framework of the explicit formulation should converge without any saturation error. We showed it did. However, we can include in the Supplementary Material of the paper a description of the vectorization for the implicit implementation if needed. But up to now, we decided not to include any description of an implicit MPM implementation. We prefer to directly refer to the relevant literature.

Change # 4 (L111-118) Additionally, we implemented a CPDI/CPDI2q version (in an explicit and quasi-static implicit formulation) of the solver. However, in this paper, we do not present the theoretical background of the CPDI variant nor the implicit implementation of a MPM-based solver. Therefore, interested readers are referred to the original contributions of Sadeghirad et al. (2013, 2011) and Acosta et al. (2020); Charlton et al. (2017); Iaconeta et al. (2017); Beuth et al. (2008); Guilkey and Weiss (2003), respectively. Regarding the quasi-static implicit implementation, we strongly adapted our vectorisation strategy to some aspects of the numerical implementation proposed by Coombs and Augarde (2020) in the MATLAB code AMPLE v1.0. However, we did not consider blocking, because our main concern for performance is on the explicit implementation.

Comment # 5 CPDI2 methods suffer from issues associated with domain distortion and are not suitable for problems involving large shear/rotation. This point should be acknowledged, see for example: Wang, L., Coombs, W.M., Augarde, C.E., Cortis, M., Charlton, T.J., Brown, M.J., Knappett, J., Brennan, A., Davidson, C., Richards, D. & Blake, A. (2019). On the use of domain-based material point methods for problems involving large distortion. *Computer Methods in Applied Mechanics and Engineering* 355: 1003-1025.

Reply # 5 It is true that CPDI2q suffers from domain distortion, as shown in the cited reference by the referee. We clarified this in the revised manuscript by introducing a new subsection "2.2 Domain-based material point method variants" (L119). In general, we discussed in greater details advantages and flaws of domain-based MPM.

Change # 5 (L120-151) Domain-based material point method variants could be treated as two distinct groups:

- The material point's domain is a square for which the deformation is always aligned with the mesh axis, i.e., a non-deforming domain uGIMP (Bardhan and Kober, 2004) or, a deforming domain cpGIMP (Wallstedt and Guilkey, 2008), the latter being usually related to a measure of the deformation, e.g., the determinant of the deformation gradient.
- The material point's domain is either a deforming parallelogram for which its dimensions are specified by two vectors, i.e., CPDI (Sadeghirad et al., 2011), or a deforming quadrilateral solely defined by its corners, i.e., CPDI2q (Sadeghirad et al., 2013). However, the deformation is not necessarily aligned with the mesh anymore.

We first focus on the different domain updating methods for GIMPM. Four domain updating methods exists: i) the domain is not updated, ii) the deformation of the domain is proportional to the determinant of the deformation gradient $\det(F_{ij})$ (Bardenhagen and Kober, 2004), iii) the domain lengths l_p are updated accordingly to the principal component of the deformation gradient F_{ii} (Sadeghirad et al., 2011) or, iv) are updated with the principal component of the stretch part of the deformation gradient U_{ii} (Charlton et al., 2017). Coombs et al. (2020) highlighted the suitability of generalised interpolation domain updating methods accordingly to distinct deformation modes. Four different deformation modes were considered by Coombs et al. (2020): simple stretch, hydrostatic compression/extension, simple shear and, pure rotation. Coombs et al. (2020) concluded the following:

- Not updating the domain is not suitable for simple stretch and hydrostatic compression/extension.
- A domain update based on $\det(F_{ij})$ will results in an artificial contraction/expansion of the domain for simple stretch.
- The domain will vanish with increasing rotation when using F_{ii} .
- The domain volume will change under isochoric deformation when using U_{ii} .

Consequently, Coombs et al. (2020) proposed a hybrid domain update inspired by CPDI2q approaches: the corners of the material point domain are updated accordingly to the nodal deformation but, the midpoints of the domain limits are used to update domain lengths l_p to maintain a rectangular domain. Even tough Coombs et al. (2020) reported an excellent numerical stability, the drawback is to compute specific basis functions between nodes and material point's corners, which has an additional computational cost. Hence, we did not selected this approach in this contribution.

Regarding the recent CPDI/CPDI2q, Wang et al. (2019) investigated the numerical stability under stretch, shear and torsional deformation modes. CPDI2q was found to be erroneous in some case, especially when torsion mode is involved, due to distortion of the domain. In contrast, CPDI and even sMPM performed better in modelling torsional deformations. Even tough CPDI2q can exactly represent the deformed domain (Sadeghirad et al., 2013), care must be taken when dealing with very large distortion, especially when the material has yielded, which is common in geotechnical engineering (Wang et al., 2019).

Consequently, the domain-based method as well as the domain updating method should be carefully chosen accordingly to the deformation mode expected for a given case. The latter will be always specify in the following and, the domain update method will be clearly stated.

Comment # 6 What large deformation formulation has been used in this paper in terms of stresses and strains? Logarithmic strains and Kirchhoff stresses? Explain and justify the large deformation framework.

Reply # 6 The large deformation formulation is based on the Jaumann stress rate formulation. It is a widely accepted deformation framework, see Huang et al. (2015); Bandara et al. (2016); Wang et al. (2016c,b) and many others. We think for an explicit implementation with a sufficiently small time step, such deformation formulation stands to reason. As such, we introduced a specific subsection "3.1 Rate formulation and elasto-plasticity".

Change # 6 (L156-163) The large deformation framework in a linear elastic continuum requires an appropriate stress-strain formulation. One approach is based on the finite deformation framework, which relies on a linear relationship between elastic logarithmic strains and Kirchhoff stresses (Coombs et al., 2020; Gaume et al., 2018; Charlton et al., 2017). In this study, we adopt another approach, namely, a rate dependent formulation using the Jaumann stress rate (e.g. Huang et al. 2015; Bandara et al. 2016; Wang et al. 2016c,b). This formulation provides an objective (invariant by rotation or frame-indifferent) stress rate measure (de Souza Neto et al., 2011) and is simple to implement. The Jaumann rate of the Cauchy stress is defined as

$$\frac{\mathcal{D}\sigma_{ij}}{\mathcal{D}t} = \frac{1}{2}C_{ijkl} \left(\frac{\partial v_l}{\partial x_k} + \frac{\partial v_k}{\partial x_l} \right), \quad (1)$$

where C_{ijkl} is the fourth rank tangent stiffness tensor and v_k is the velocity. Thus, the Jaumann stress derivative can be written as

$$\frac{\mathcal{D}\sigma_{ij}}{\mathcal{D}t} = \frac{D\sigma_{ij}}{Dt} - \sigma_{ik}\omega_{jk} - \sigma_{jk}\omega_{ik}, \quad (2)$$

where $\omega_{ij} = (\partial_i v_j - \partial_j v_i)/2$ is the vorticity tensor and $D\sigma_{ij}/Dt$ denotes the material derivative

$$\frac{D\sigma_{ij}}{Dt} = \frac{\partial \sigma_{ij}}{\partial t} + v_k \frac{\partial \sigma_{ij}}{\partial x_k}. \quad (3)$$

Comment # 7 How has the plasticity algorithm been implemented within the large deformation framework? The authors mention a prediction/correction type algorithm so how have they recovered the additive decomposition of the elastic and plastic strains from the multiplicative decomposition of the deformation gradient? Critical details are missing here.

Reply # 7 It is true that critical details are missing concerning the plasticity algorithm we selected. We added more details concerning the way plasticity is handle in the revised manuscript. More specifically, we used the prediction/correction algorithm combined with the Jaumann stress rate formulation which allow us to afford the decomposition of the elastic and plastic strain from the decomposition of the deformation gradient, as done in the MATLAB code AMPLE. We present in detail the general implementation of plastic flow accordingly to Simpson (2017) in the subsection "3.1 Rate formulation and elasto-plasticity".

Change # 7 (L164-184) Plastic deformation is modelled with a pressure dependent Mohr-Coulomb law with non-associated plastic flow, i.e., both the dilatancy angle ψ and the volumetric plastic strain ϵ_v^p are null (Vermeer and De Borst, 1984). We have adopted the approach of Simpson (2017) for a two dimensional linear elastic, perfectly plastic (elasto-plasticity) continuum because of its simplicity and its ease of implementation. The yield function is defined as

$$f = \tau + \sigma \sin \phi - c \cos \phi, \quad (4)$$

where c is the cohesion and ϕ the angle of internal friction,

$$\sigma = (\sigma_{xx} + \sigma_{yy})/2, \quad (5)$$

and

$$\tau = \sqrt{(\sigma_{xx} - \sigma_{yy})^2/4 + \sigma_{xy}^2}. \quad (6)$$

The elastic state is defined when $f < 0$. However when $f > 0$, plastic state is declared and stresses must be corrected (or scaled) to satisfy the condition $f = 0$, since $f > 0$ is an inadmissible state. Simpson (2017) proposed the following simple algorithm to return stresses to the yield surface,

$$\sigma_{xx}^* = \sigma + (\sigma_{xx} - \sigma_{yy})\beta/2, \quad (7)$$

$$\sigma_{yy}^* = \sigma - (\sigma_{xx} - \sigma_{yy})\beta/2, \quad (8)$$

$$\sigma_{xy}^* = \sigma_{xy}\beta, \quad (9)$$

where $\beta = (|c \cos \phi - \sigma \sin \phi|)/\tau$, and σ_{xx}^* , σ_{yy}^* and σ_{xy}^* are the corrected stresses, i.e., $f = 0$.

A similar approach is used to return stresses when considering a non-associated Drucker-Prager plasticity (see Huang et al. (2015) for a detailed description of the procedure). In addition, their approach allows also to model associated plastic flows, i.e., $\psi > 0$ and $\epsilon_v^p \neq 0$.

Comment # 8 How are boundary conditions imposed in this model?

Reply # 8 Boundary conditions can be difficult to impose thoroughly in MPM, especially when considering non-aligned boundary conditions with respect to the background mesh, as mentioned in Cortis, M., Coombs, W., Augarde, C., Brown, M., Brennan, A., Robinson, S. Imposition of essential boundary conditions in the material point method. International Journal for Numerical Methods in Engineering. 113: 130-152. This is the main reason why we choose numerical problem and setup in which boundary conditions could be directly applied on the background mesh. We mentioned this important point of aligned boundary conditions in the revised manuscript in the new subsection "3.4 Initial settings and adaptive time step".

Change # 2 (L315-319) In this contribution, Dirichlet boundary conditions are resolved directly on the background mesh, as in the standard finite element method. This implies that boundary conditions are resolved only in contiguous regions between the mesh and the material points. Deviating from this contiguity or having the mesh not aligned with the coordinate system requires specific treatments for boundary conditions (Cortis et al., 2018). Furthermore, we ignore the external tractions as their implementation is complex.

Comment # 9 Figure 6 - what causes the step in the red line around 10^3 material points? Is there a shift in terms of the cost within the algorithm?

Reply # 9 Thank you for this comment. We started an investigation in terms of flops and L2 cache concerning this step around 10^3 material points and we just concluded this shift is due to the overhead and RAM-to-cache transfer. As mentioned further by the referee, overheads are a major concern in MATLAB. This step typically occurs when the block of data sent from RAM to the CPU L2 cache exceeds its maximum capacity. MATLAB can no longer treat the information as a contiguous block of data sent once and start swapping from RAM to cache and back and forth. This costs an additional computational expense which results in this step in Fig. 6 in the original paper (see 1).

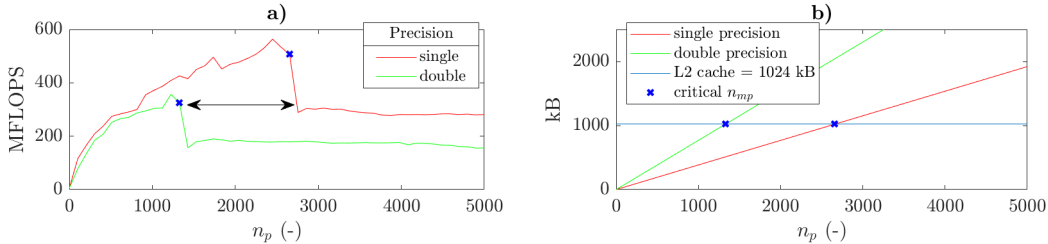


Figure 1: a) Floating-point operation per second in million and, b) linear increase of RAM usage with an increasing number of material point. The limit when the allocated space in RAM reaches the L2 cache size (1024kB) corresponds to the drop of FLOPS in FIG I a).

Thanks to the referees comment, we now come with a different approach to vectorise the matrix multiplication problem which is faster than the previous one but still suffers from overhead due RAM-to-cache communication. For this particular problem, we report a rather significant difference between the two vectorisation variants. This is particularly obvious when we observe the difference in terms of Mflops: flops are at least twice higher than the former implementation for the matrix multiplication (see Fig. 2). In the earlier version of the solver, the matrix multiplication problem was handle by the MATLAB instruction depicted in line 6 in the code listing 1. However, the function `permute()` is less efficient than using the function `reshape()`. Hence, we found out it was more efficient to use the MATLAB instruction in line 8 in the code listing 1 instead. However, these two variants give the exact same result as the standard iterative matrix multiplication in line 3 in the code listing 1.

Even tough it does not ensure optimal RAM-to-cache communications, it increased rather significantly the performance compared to the previous version. Consequently, we replaced the previous vectorisation by this new technique and make the necessary changes in our revised paper. It also implied to modify results and observations in the computational efficiency section of the paper. Therefore, the actual version of the solver is v1.1. This has been changed wherever necessary in the revised manuscript. However, we also

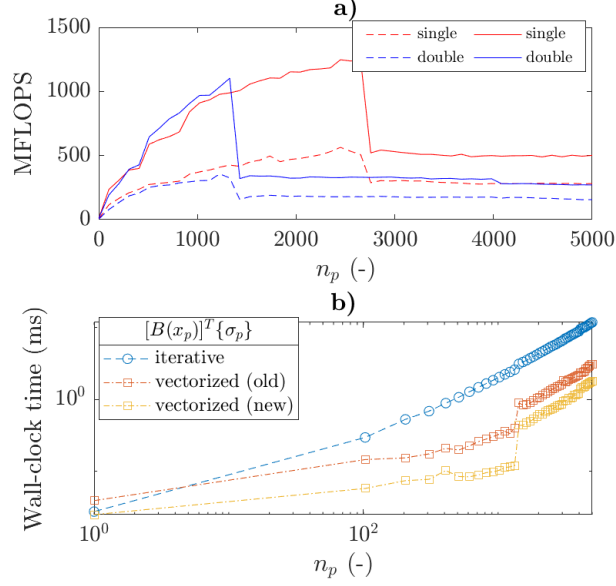


Figure 2: a) Floating-point operation per second (in million) for old (dashed lines) and new (continuous lines) vectorisation frameworks and, b) wall-clock time (in ms) for an increasing number of material point n_p for an iterative calculation, the old and the new vectorisation frameworks.

mentioned the drop of efficiency due to overheads. In addition, this computational cost due to RAM-to-cache communication would be an interesting improvement of a future implementation of a vectorised MPM code in MATLAB.

```

1 %% MATRIX MULTIPLICATION USING FOR LOOP
2 for k = 1:np(p)
3     loop_Bs(:,k) = (B(:, :, k))'*(s(:, k))
4     ;% matrix multiplication operator *
5 end
6 %% MATRIX-VECTOR MULTIPLICATION USING VECTORISATION
7 vect_Bs = squeeze(sum(permute(B, [2 1 3]).*...
8     repmat((permute(s', [3 2 1])), nDoF, 1), 2))
9     ;% old matrix-vector multiplication
10 vect_Bs = (squeeze(sum(B.*repmat(reshape(s, 3, 1, np(p)), 1, nDoF)
11     , 1))) ;% new matrix-vector multiplication

```

Listing 1: Original (v1.0) and new (v1.1) vectorised solutions of the matrix multiplication problem.

Change # 9 (L281-288) To illustrate the numerical efficiency of the vectorised multiplication between a matrix and a vector, we have developed an iterative and vectorised solution of $\mathbf{B}(\mathbf{x}_p)^T \boldsymbol{\sigma}_p$ with an increasing n_p and considering single (4 bytes) and double (8 bytes) arithmetic precision. The wall-clock time increases with n_p with a sharp transition for the vectorised solution around $n_p \approx 1000$, as showed in Fig 6a. The mathematical operation requires more memory than available in the L2 cache (1024 kB under the CPU architecture used), which inhibits cache reuse (Dabrowski et al., 2008). A peak performance of at least 1000 Mflops, showed in Fig. 6b, is achieved when $n_p = 1327$ or $n_p = 2654$ for simple or double arithmetic precision respectively, i.e., it corresponds exactly to 1024 kB for both precisions. Beyond, the performance dramatically drops to approximately the half of the peak value. This drop is even more severe for a double arithmetic precision.

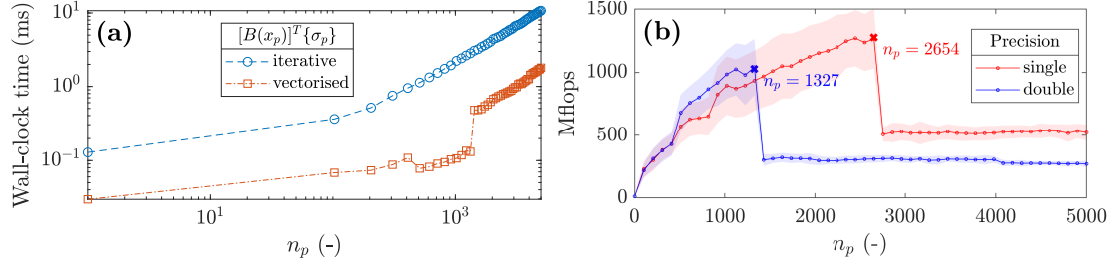


Figure 6: a) Wall-clock time to solve for a matrix multiplication between a multidimensional array and a vector with an increasing number of the third dimension with a double arithmetic precision and, b) number of floating point operations per second (flops) for single and double arithmetic precisions. The continuous line represents the averages value whereas the shaded area denotes the standard deviation.

Comment # 10 It is well known that MPMs can provide a reasonable global approximation (in terms of force-displacement response) but the computed stress field can be spurious/highly oscillatory due to issues such as locking and/or cell crossing. The authors should present the predicted stress response for the numerical examples presented in the paper and compare them to analytical solutions where available.

Reply # 10 This is a good suggestion. We present the stress field for selected numerical problems in the revised manuscript, i.e., the elastic compression and the cantilever beam. Additionally, we also present the analytical solution of the stress σ_{yy} for the elastic column and its analytical solution.

Change # 10

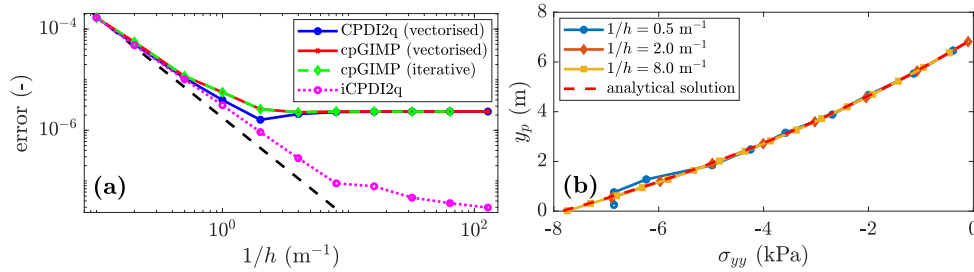


Figure 9: a) Convergence of the error: a limit is reached at error $\approx 2 \cdot 10^{-6}$ for the explicit solver, whereas the quasi-static solution still converges. This was already demonstrated in Bardenhagen and Kober (2004) as an error saturation due to the explicit scheme, i.e., the equilibrium is never resolved. b) The stress σ_{yy} along the y -axis predicted at the deformed position y_p by the CPDI2q variant is in good agreements with the analytical solution for a refined mesh.

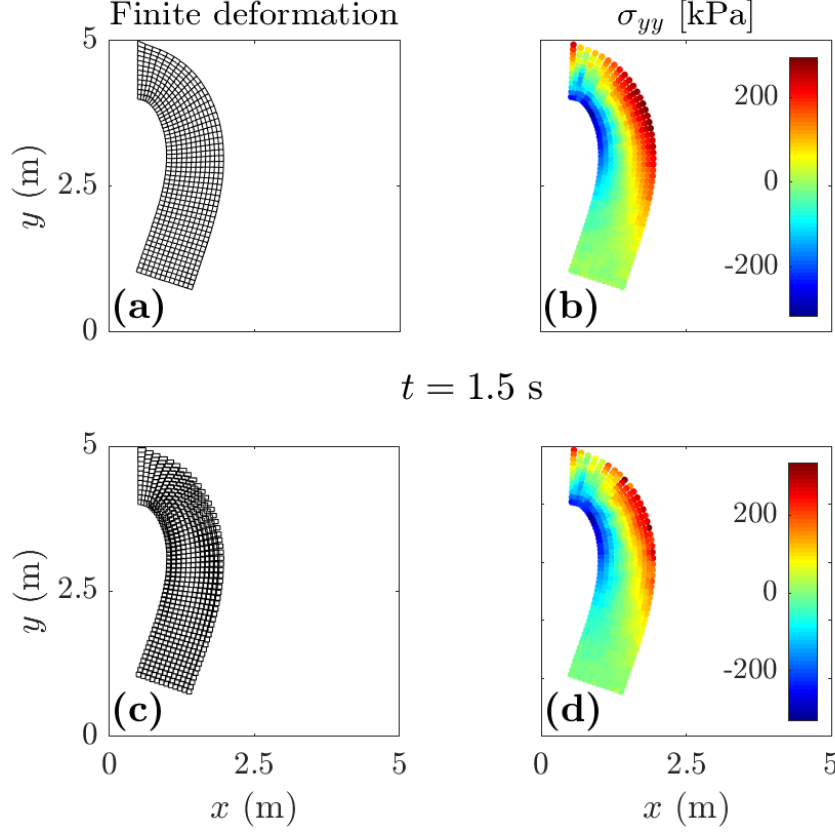


Figure 13: Finite deformation of the material point domain and vertical Cauchy stress σ_{yy} for CPDI, i.e., a) & b), and for cpGIMP, i.e., c) & d). The CPDI variant gives a better and contiguous description of the material point's domain and a slightly smoother stress field, compared to the cpGIMP variant, which is based on the stretch part of the deformation gradient.

Comment # 11 The elastic column problem will only have around 2 % deformation in terms of the deformed to original height so this problem is not a good test of the convergence of MPMs. The authors refer to the work of Coombs et al. for this problem but they show convergence for the case where the column compresses to around 50 % of its initial height. Run the convergence for the case with a Young's modulus of 10kPa, not 1MPa.

Reply # 11 The referee is right; the elastic column will only have a small vertical deformation. We run the convergence analysis with lower elastic modulus as proposed to achieve a greater deformation of the column.

Change # 11 (L360-361) The material has a Young's modulus $E = 1 \cdot 10^4$ Pa and a Poisson's ratio $\nu = 0$ with a density $\rho = 80 \text{ kg m}^{-3}$.

Comment # 12 How have the authors avoided volumetric locking when using isochoric plastic flow? What do the pressure distributions look like through the deformed domains?

Reply # 12 We did not avoid volumetric locking when using isochoric plastic flow. As a result, the pressure field experience severe oscillations for isochoric plastic deformations. It is true that any MPM variant suffers from volumetric locking. As such, we now clearly state in the revised manuscript that we did not treat the oscillation of the pressure field due to volumetric locking. We also discuss in detail the issue of volumetric locking in the Discussion section and share potential ways to regularize the pressure field, especially when isochoric plastic deformations are involved.

Change # 12 (L513-517) This particular case of isochoric plastic deformations rises the issue of volumetric locking. In the actual implementation, no regularization techniques are considered. As a result, the pressure field experience severe locking for isochoric plastic deformations. One way to overcome locking phenomenons would be to implement the regularization technique initially proposed by Coombs et al. (2018) for quasi-static sMPM and GIMPM implementations.

Comment # 13 The various comments on the use of cpGIMP and uGIMP are confused and misleading. Just because an analysis is stable it does not mean that it is "appropriate" as the results may be meaningless. The authors cite the work of Coombs to justify the use of the stretch to update the domains, however this technique does not work for problems involving simple shear type deformation, refer to Table 2 of: Coombs, WM, Augarde, CE, Brennan, AJ, Brown, MJ, Charlton, TJ, Knappett, JA, Ghaffari Motlagh, Y & Wang, L (2020). On Lagrangian mechanics and the implicit material point method for large deformation elasto-plasticity. Computer Methods in Applied Mechanics and Engineering 358: 112622. The authors later adopt a determinant of the deformation gradient-type updating method but this has been shown to not converge for simple compression problems as the domains artificially shrink in the non-compressed direction and overlap in the compressed direction (see Figure 8 from the above reference). For example, the statement on lines 76-77 is not correct, or rather it is only correct for some types of problem.

Reply # 13 We agree that this various comment all around the manuscript were confused and misleading. As such, we elaborated the presentation of domain-based MPMs and correctly refer to advantages and flaws for each of these domain-based variants. Consequently, we included a new subsection in the MPM overview section, e.g., "2.2 Domain-based material point method variants".

Regarding the determinant of the deformation gradient-type update, the referee comment is absolutely true. However, we selected such approach since it gave the most stable numerical result. But, we clearly mentioned the problem of artificial shrinking and domain overlaps associated with this variant in the revised paper.

Change # 14 See Change # 5.

Comment # 14 The speed gains of MILAMIN come from the combination of blocking and vectorisation. Have both techniques been used in this paper? If so, what are the relative speed gains from the different sources? How does the speed gain change with different block sizes?

Reply # 14 We did use vectorisation but we did not use blocking. It is true that in MILAMIN the speed gain come from a combination between vectorisation and blocking. However, such technique is applied in assembling local stiffness matrix in the global stiffness matrix, which does not appear in an explicit MPM formulation. Hence, the technique of blocking was disregarded for that concern. We acknowledge this statement in the introduction section.

Change # 14 (L64-67) We did not consider the blocking technique initially proposed by Dabrowski et al. (2008) since an explicit formulation in MPM excludes the global stiffness matrix assembly procedure. The performance gain mainly comes from the vectorisation of the algorithm, whereas blocking has a less significant impact over the performance gain, as stated by Bird et al. (2017).

Comment # 15 The authors have not explained by MATLAB is inefficient when working with small amounts of data. This point should be discussed with reference to CPU cache size and RAM-to-cache overheads.

Reply # 15 We discussed this point explicitly when presenting the new vectorisation framework of the matrix multiplication problem we mentioned previously in our response. In addition, we also discuss this issue in the section "5. Discussion".

Change # 15 (L37-39) Hence, mathematical operations over a large number of small matrices should be avoided and, operations on fewer and larger matrices preferred. This is a typical bottleneck in FEM when local stiffness matrices are assembled during the integration point loop within the global stiffness matrix.

(L284-285) The mathematical operation requires more memory than available in the L2 cache (1024 kB under the CPU architecture used), which inhibits cache reuse (Dabrowski et al., 2008).

(538-542) An iterative implementation would require multiple nested for-loops and a larger number of operations on smaller matrices, which increase the number of BLAS calls, thus inducing significant BLAS overheads and decreasing the overall performance of the solver. This is limited by a vectorised code structure. However and as showed by the matrix multiplication problem, the L2 cache reuse is the limiting factor and, it ultimately affects the peak performance of the solver due to these numerous RAM-to-cache communications for larger matrices.

Comment # 16 It would be more appropriate to present the speed gains in terms of flops. There should be a peak in performance if you consider large enough problems.

Reply # 16 Thank you for this relevant suggestion. As mentioned previously in our reply, we already started to investigate the speed gain of the matrix-vector operation problem. We extended this point to our computational performance analysis, which greatly benefited from this. Our performance analysis focused on both the number of iterations per second and the number of floating-point operations per second with respect to the total number of material points. As stated by the referee, a peak performance is reached and then, a residual performance is further resolved as the total number of material points increases.

Change # 16 (L473-482) The performance of the solver is demonstrated in Fig. 18. A peak performance of ≈ 900 Mflops is reached, as soon as n_p exceeds 1000 material points and, a residual performance of ≈ 600 Mflops is further resolved (for n_p approximately 50000 material points). Every functions provide an even and fair contribution on the overall performance, except the function `constitutive.m` for which the performance appears delayed or shifted. First of all, this function treats the elasto-plastic constitutive relation, in which the dimensions of the matrices are smaller when compared to the other functions. Hence, the amount of floating point operations per second is lower compared to other functions, e.g., `p2Nsolve.m`. This results in less performance for an equivalent number of material points. It also requires a greater number of material points to increase the dimensions of the matrices in order to exceed the L2 cache maximum capacity.

This considerations provide a better understanding of the performance gain of the vectorised solver showed in Fig. 19: the gain increases and then, reaches a plateau and ultimately, decreases to a residual gain. This is directly related to the peak and the residual performances of the solver showed in Fig. 18.

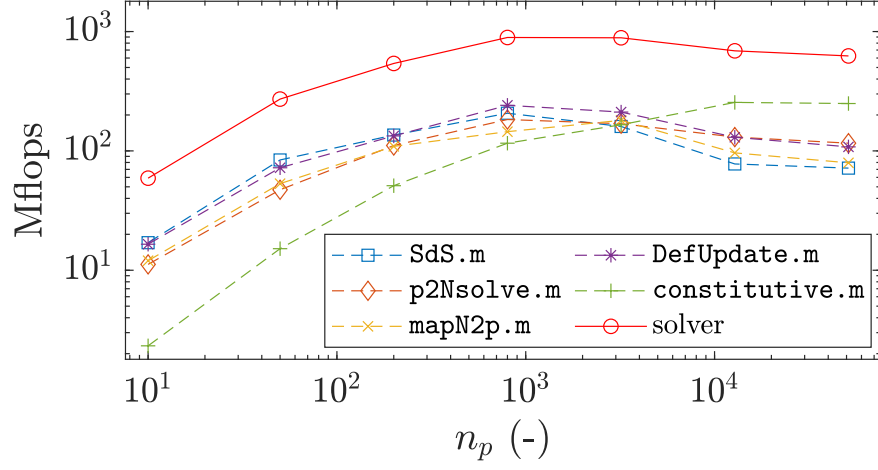


Figure 18: Number of floating point operation per seconds (flops) with respect to the total number of material point n_p for the vectorised implementation. The discontinuous lines refer to the functions of the solver, whereas the continuous line refer to the solver. A peak performance of 900 Mflops is reached by the solver for $n_p > 1000$ and, a residual performance of 600 Mflops is further resolved for an increasing n_p .

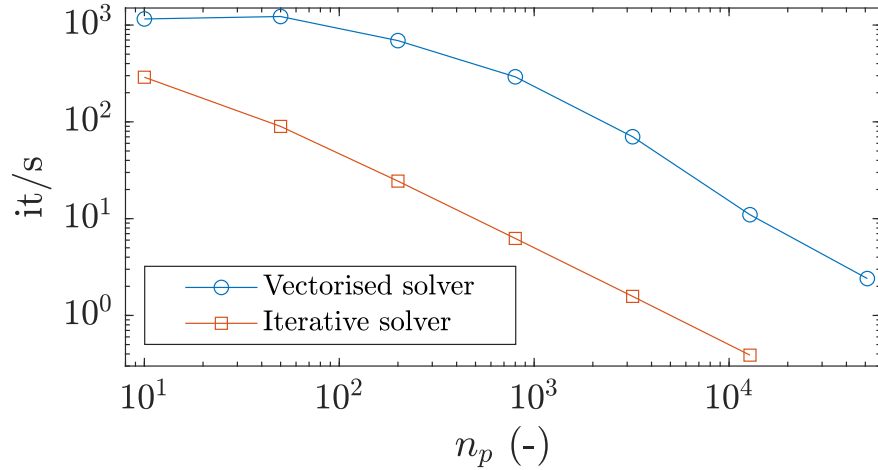


Figure 19: Number of iterations per second with respect to the total number of material point n_p . The greatest performance gain is reached around $n_p = 1000$, which is related to the peak performance of the solver (see Fig. 18). The gains corresponding to the peak and residual performances are 46 and 28 respectively.

Comment # 17 Figure 2 is misleading as the GIMP domain is fully inside a single element and will have the same connectivity as the standard MP case.

Reply # 17 We agree that Figure 2 was misleading. Consequently, we replaced the previous Figure 2 by a new one in the revised manuscript. In addition, we also included the nodal connectivity for the CPDI2q variant.

Change # 17

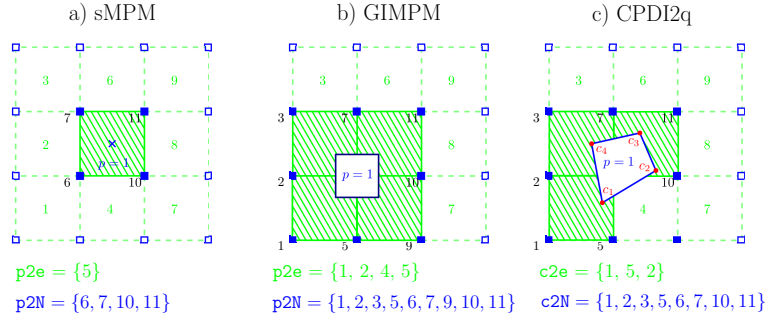


Figure 2: Nodal connectivities of a) standard MPM, b) GIMP and c) CPDI2q variants. The material point's location is marked by the blue cross. Note that for sMPM (and similarly BSMPM) the particle domain does not exist, unlike GIMP or CPDI2q (the blue square enclosing the material point). Nodes associated with the material point are denoted by filled blue squares, and the element number appears in green in the centre of the element. For sMPM and GIMP, the connectivity array between the material point and the element is $p2e$ and, the array between the material point and its associated nodes is $p2N$. For CPDI2q, the connectivity array between the corners (filled red circles) of the quadrilateral domain of the material point and the element is $c2e$ and, the array between the corners and their associated nodes is $c2N$.

Comment # 18 Line 162 - the authors mention a 30 % speed up - what problem/size of problem/number of points, etc?

Reply # 18 We mentioned a 30 % speed up at Line 162 in the original manuscript for the calculation of the shape function. We carried out a more thoroughly analysis of such speed up and observe a steady gain regardless of the number of material points or the number of element. Consequently, we simply mention this within the text. However, we also noted the sentence was not clear enough. Therefore, we made our point more straight forward in indicating that such speed up was only valid for the calculation of the shape function during a computational cycle and not over the whole solver.

Change # 18 (L247-249) The performance gain is significant between the two approaches, i.e., an intrinsic 30 % gain over the wall-clock time of the basis functions and derivatives calculation. We observe an invariance of such gain with respect to the initial number of material point per element or to the mesh resolution.

Comment # 19 Where are material points located within the elements when the problems are set up?

Reply # 19 Regarding the initial location of material points within elements, we preferred a regular distribution of material point within elements. Considering 4 material points per element, their location (in local coordinate) would be $[-0.5; 0.5]$ along x and y direction. Hence, we decided to simply mention that we only consider a regular mesh spacing with a uniform distribution of material points per initially populated element. As suggested by the second referee, this was included in the new subsection "3.3 Initial settings and adaptive time step".

Change # 19 (L312-314) Regarding the initial setting of the background mesh of the demonstration cases further presented, we select a uniform mesh and a regular distribution of material points within the initially populated elements of the mesh. Each element is evenly filled with 4 material points, e.g., $n_{pe} = 2^2$, unless otherwise stated.

Comment # 20 Some key information is missing from the numerical analysis, such as time step sizes and total times which would make it impossible to reproduce the results. This information must be added.

Reply # 20 During the revision process of our contribution, we decided to consider an adaptive time step. Hence, we clearly mention this in the revised manuscript and we provide the reader with the CFL number C we used for every demonstration case. Whenever relevant, we also mention the minimal and maximal time steps obtained given elastic properties of the material and the CFL number chosen and we also specify the total simulation time.

Change # 20 (L320-328) As explicit time integration is only conditionally stable, any explicit formulation requires a small time step Δt to ensure numerical stability (Ni and Zhang, 2020), e.g., smaller than a critical value defined by the Courant-Friedrich-Lewy (CFL) condition. Hence, we employ an adaptive time step (de Vaucorbeil et al., 2020), which considers the velocity of the material points. The first step is to compute the maximum wave speed of the material using (Zhang et al., 2016; Anderson Jr, 1987)

$$(c_x, c_y) = \{\max_p(V + |(v_x)_p|), \max_p(V + |(v_y)_p|)\}, \quad (10)$$

where the wave speed is $V = ((K + 4G/3)/\rho)^{\frac{1}{2}}$, K and G are the bulk and shear moduli respectively, ρ is the material density, $(v_x)_p$ and $(v_y)_p$ are the material point velocity components. Δt is then restricted by the CFL condition as followed:

$$\Delta t = \alpha \min \left(\frac{h_x}{c_x}, \frac{h_y}{c_y} \right), \quad (11)$$

where $\alpha \in [0; 1]$ is the time step multiplier, and h_x and h_y are the mesh spacings.

Comment # 21 Incomplete sentence on line 359.

Reply # 21 That is correct, sentence on line 359 was completed in the revised manuscript.

Change # 21 (L497-498) In this contribution, a fast and efficient explicit MPM solver is proposed that considers two variants (e.g., the uGIMPM/cpGIMPM and the CPDI/CPDI2q variants).

2 Referee #2

This manuscript presents a vectorized material point method for MATLAB and quantifies the increase in computational efficiency gained from using vectorized rather than iterative code. To my knowledge, this paper provides the only formal analysis of the performance gains from vectorizing MPM code. The presented vectorization approach could be easily implemented within existing and future MPM models. However, as already thoroughly noted by Referee #1, many details of the algorithms, setup of simulations, and numerical analysis are missing. I would like to add the following comments to those already given.

Comment # 1 I found the structure of the paper to be confusing, especially in Section 4, where results from five test cases are reported. These test cases are all nearly exact reproductions of previously-published work. The first two test cases – the elastic compaction of a column (Section 4.1) and elastic cantilever beam (Section 4.2) – appear to solely serve as benchmark examples for verification of the MPM model, though this is not clearly stated. The third test case – elasto-plastic column collapse (Section 4.3) – also appears to serve as further verification of the model until it is used again in Section 4.4, where the main results of the paper concerning the computational efficiency gained from vectorization are presented. A fourth test case (collision

of two elastic disks) is also presented in 4.4 for further analysis of computational efficiency. The final test case (elasto-plastic landslide) is then presented in Section 4.5, which seems to serve the dual purpose of further model verification and a geomechanical application.

Reply # 1 It is true that the structure might be confusing. We focus on the section "4. Results" and made our point clearer by adding, as suggested in the following by the referee, a quick introduction to this section. We think it improves the readability of this section.

Overall, the reorganised section "4. Results" now reads as:

1. Results

- (a) Validation of the solver and numerical efficiency
 - i. Convergence: elastic compaction under self-weight of a column
 - ii. Large deformation: the elastic cantilever beam problem
 - iii. Application: the elasto-plastic slumpin dynamics
- (b) Computational performance
 - i. Iterative and vectorised elasto-plastic collapses
 - ii. Comparison between Julia and MATLAB

We also clearly state our motivation of the exact reproduction of previously-published works. We think it is also important to showcase the efficiency of our solver with benchmarks from past studies. However, we reorganized the subsection in which computational performances are showed, in order to make our point more obvious to the reader.

Change # 1 (L330-344) In this section, we first demonstrate our MATLAB-based MPM solver to be efficient in reproducing results from other studies, i.e., the compaction of an elastic column (Coombs et al., 2020) (e.g., quasi-static analysis), the cantilever beam problem (Sadeghirad et al., 2011) (e.g., large elastic deformation) and an application to landslide dynamics (Huang et al., 2015) (e.g., elasto-plastic behaviour). Then, we present both the efficiency and the numerical performances for a selected case, e.g., the elasto-plastic collapse. We conclude and compare the performances of the solver with respect to the specific case of an impact of two elastic disks previously implemented in a Julia language environment by (Sinaie et al., 2017).

Regarding the performance analysis, we investigate the performance gain of the vectorised solver considering a double arithmetic precision with respect to the total number of material point because of the following reasons: i) the mesh resolution, i.e., the total number of elements n_{el} , influences the wall-clock time of the solver by reducing the time step due to the CFL condition hence increasing the total number of iterations. In addition, ii) the total number of material points n_p increases the number of operations per cycle due to an increase of the size of matrices, i.e., the size of the strain-displacement matrix depends on n_p and not on n_{el} . Hence, n_p consistently influences the performance of the solver whereas n_{el} determines the wall-clock time of the solver. The performance of the solver is addressed through both the number of floating point operations per second (flops), and by the average number of iteration per second (it/s). The number of floating point operations per second was manually estimated for each function of the solver.

Comment # 2 The motivation behind most of the test cases is not clear, especially on the first read. Section 4 would benefit from a short introduction (before 4.1) that outlines what test cases were selected and for what purpose.

Reply # 2 Thank you for this comment. We agree that the motivation behind most of the test cases is not clear. Consequently, we have now written two paragraphs (as a preamble) at the very beginning of the section "4. Results" in which we clearly state our motivations of i) reproducing efficiently results from other studies and ii) analyse the computational performance of our solver for two selected cases, i.e., the elasto-plastic granular collapse and the elastic disk impact problem.

Change # 2 See Change # 1

Comment # 3 It may help readability if the test cases for elasto-plastic column collapse and collision of two elastic disks are separated into an entirely different section from the rest of the examples, as these two test cases provide the main results in the paper regarding the computational efficiency gained by vectorization.

Reply # 3 It is a good suggestion and it should even significantly help the readability of the manuscript. We created a new subsection "4.2 Computational performance" composed of two subsubsections, namely "4.2.1 Iterative and vectorised elasto-plastic collapses" and "4.2.2 Comparison between Julia and MATLAB".

Change # 3 See Reply # 1 and Change # 1

Comment # 4 Many of the statements regarding the effectiveness of cpGIMPM vs. uGIMPM vs. CPDI are misleading or lacking in detail:

Reply # 4 We agree with the Referee that the statements related to the effectiveness of uGIMPM, cpGIMPM and CPDI are misleading or lacking in detail. Therefore, we created a new subsection "2.2 Domain-based material point method variants", which summarises the major difference between GIMPM and CPDI (the way the material points domain is updated). We also present the different domain updating methods for GIMPM and we more clearly highlight the suitability of each of these domains updating methods based on the investigation of Coombs, WM, Augarde, CE, Brennan, AJ, Brown, MJ, Charlton, TJ, Knappett, JA, Ghaffari Motlagh, Y & Wang, L (2020). On Lagrangian mechanics and the implicit material point method for large deformation elasto-plasticity. Computer Methods in Applied Mechanics and Engineering 358: 112622, and, Wang, L., Coombs, W.M. , Augarde, C.E. , Cortis, M. Charlton, T.J. , Brown, M.J. Knappett, J., Brennan, A. Davidson, C. Richards, D. & Blake, A. (2019). On the use of domain-based material point methods for problems involving large distortion. Computer Methods in Applied Mechanics and Engineering 355: 1003-1025. Finally, we explicitly state at the end of new 2.2 subsection that the domain-based method as well as the domain update method should be carefully chosen accordingly to the deformation mode expected for a given case. Moreover, the domain update method is clearly stated in each case presented in the section "5. Results". We believe that now this additional 2.2 subsection provides a better overview of both domain-based method and domain updating method.

Change # 4 See Change # 5 for the first referee

Comment # 5 Line 288: in what way did domain updates based on the deformation gradient result in failure?

Reply # 5 The domain updates based on the deformation gradient showed some flaws of GIMP-based implementation, i.e. the domain artificially shrinks under large rotation, which was already demonstrated in Fig.4 in Coombs, WM, Augarde, CE, Brennan, AJ, Brown, MJ, Charlton, TJ, Knappett, JA, Ghaffari Motlagh, Y & Wang, L (2020). On Lagrangian mechanics and the implicit material point method for large deformation elasto-plasticity. Computer Methods in Applied Mechanics and Engineering 358: 112622. We now clearly mention the reason why the simulation in which the domain updates based on the deformation gradient failed for the cantilever beam problem. In addition, we restructured the elasto-plastic collapse. Hence, we now only mentioned that we performed preliminary analyses to select the most suitable domain updating method for the cpGIMPM variant.

Change # 5 (L398-399) As indicated in Sadeghirad et al. (2011), the cpGIMPM simulation failed when using the diagonal components of the deformation gradient to update the material point domain, i.e., the domain vanishes under large rotations as stated in Coombs et al. (2020).

(L460-464) We conducted preliminary investigations using either uGIMPM or cpGIMPM variants, the latter with a domain update based either on the determinant of the deformation gradient or on the diagonal

components of the stretch part of the deformation gradient. We concluded the uGIMPM was the most reliable, even though its suitability is restricted to both simple shear and pure rotation deformation modes (Coombs et al., 2020).

Comment # 6 Line 301: [The elasto-plastic MPM solver] demonstrates the inability of the MPM variants based on a domain update (GIMPM or CPDI) to resolve extremely large plastic deformations when relying on the normal components of the deformation gradient or its stretch part to update the material point domain. This is too general of a statement. There are many cases in which these domain updates would work well; for example, if simple shear is minimal and the "stretch" update is used (Coombs et al 2020). A similarly-flawed statement is made in the conclusion section (lines 394-396). Better conclusions regarding GIMPM/CPDI might incorporate the performance gains reported using the vectorization scheme for calculation of the shape functions and the difference in computational efficiency measured for GIMPM vs CPDI.

Reply # 6 We agree that the statement on Line 301 is too general. As such, we specified our concern regarding the deformation mode involved avoiding such flawed statements in the revised version of the manuscript, referring explicitly to the work of Coombs, WM, Augarde, CE, Brennan, AJ, Brown, MJ, Charlton, TJ, Knappett, JA, Ghaffari Motlagh, Y & Wang, L (2020). On Lagrangian mechanics and the implicit material point method for large deformation elasto-plasticity. Computer Methods in Applied Mechanics and Engineering 358: 112622. As suggested by the Referee, we now focus our discussion on the performance gain of GIMPM and CPDI variants, which is indeed the main point of our contribution.

Change # 6 (L531-550) The computational performance comes from the combined use of the connectivity array `p2N` with the built-in function `accumarray()` to i) accumulate material point contributions to their associated nodes or, ii) to interpolate the updated nodal solutions to the associated material points. When a residual performance is resolved, an overall performance gain (e.g., the amount of it/s) of 28 is reported. As an example, the functions `p2nsolve.m` and `mapN2p.m` are 24 and 22 times faster than an iterative algorithm when the residual performance is achieved. The overall performance gain is in agreement to other vectorised FEM codes, i.e., OSullivan et al. (2019) reported an overall gain of 25.7 for a optimised continuous Galerkin finite element code.

An iterative implementation would require multiple nested for-loops and a larger number of operations on smaller matrices, which increase the number of BLAS calls, thus inducing significant BLAS overheads and decreasing the overall performance of the solver. This is limited by a vectorised code structure. However and as showed by the matrix multiplication problem, the L2 cache reuse is the limiting factor and, it ultimately affects the peak performance of the solver due to these numerous RAM-to-cache communications for larger matrices. Such problem is serious and, its influence is demonstrated by the delayed response in terms of performance for the function `constitutive.m`. However, we also have to mention that the overall residual performance was resolved only for a limited total number of material points. The performance drop of the function `constitutive.m` has never been achieved. Consequently, we suspect an additional decrease of overall performances of the solver for larger problems.

The overall performance achieved by the solver is higher than expected and, is even higher with respect to what was reported by Sinaie et al. (2017). We demonstrate that MATLAB is even more efficient than Julia, i.e., a minimum 2.86 performance gain achieved compared to a similar Julia CPDI2q implementation. This confirms the efficiency of MATLAB for solid mechanics problems, provided a reasonable amount of time is spent on the vectorisation of the algorithm.

Comment # 7 Line 305: As already pointed out by Referee #1, it should be noted that the determinant of the deformation gradient-type GIMPM domain update is problematic for simple compression problems. Have the authors tried updating the GIMPM domains with the corner scheme from Eqs 35-37 in Coombs et al (2020)? Perhaps it would be more robust.

Reply # 7 This is a good comment. First, we added a presentation of the suitability of domain updating methods in GIMPM for the possible deformation modes, directly referring to the work of Coombs, WM, Augarde, CE, Brennan, AJ, Brown, MJ, Charlton, TJ, Knappett, JA, Ghaffari Motlagh, Y & Wang, L

(2020). On Lagrangian mechanics and the implicit material point method for large deformation elastoplasticity. *Computer Methods in Applied Mechanics and Engineering* 358: 112622. This is important and is lacking up to now. Concerning the investigation of the corner update, we did not have tried to implement it. We decided to quickly investigate this scheme but we figured out it was necessary to compute additional shape functions between material points corners and nodes, similarly to the CPDI variant. Our concern comes from the need to compute these additional quantities, alongside to the shape function relating material points to their associated nodes. This extra cost is significant, especially when our major concern is computational performance. We therefore decided not to pursue such investigation for that reason. We discuss this in the section "5. Discussion"

Change # 7 (L526-530) We did not selected the domain updating method based on the corners of the domain as suggested in Coombs et al. (2020). This is because such domain updating method necessitates to calculate additional shape functions between the corners of the domain of the material point with their associated nodes. This results in an additional computational cost. Nevertheless, such variant is of interest and should be addressed as well when the computational performances are not the main concern.

Comment # 8 There does not appear to be any reference to Fig. 1 in the main text. The caption for Fig. 1 also appears to lack any description of panels B and C.

Reply # 8 Indeed, there was no reference to Fig. 1 in the main text. We added a description of panels B and C in the figure caption as highlighted by the referee and, we refer now to this Fig. 1 in the main text, as mentioned in the following reply # 9.

Change # 8 (L81-93) Hence, a typical calculation cycle (see Fig. 1) consists of the three following steps (Wang et al., 2016a):

1. A Mapping phase, during which properties of the material point (mass, momentum or stress) are mapped to the nodes.
2. An updated-Lagrangian FEM (UL-FEM) phase, during which the momentum equations are solved on the nodes of the background mesh and, the solution is explicitly advanced forward in time.
3. A Convection phase, during which i) the nodal solutions are interpolated back to the material points, and ii) the properties of the material point are updated.

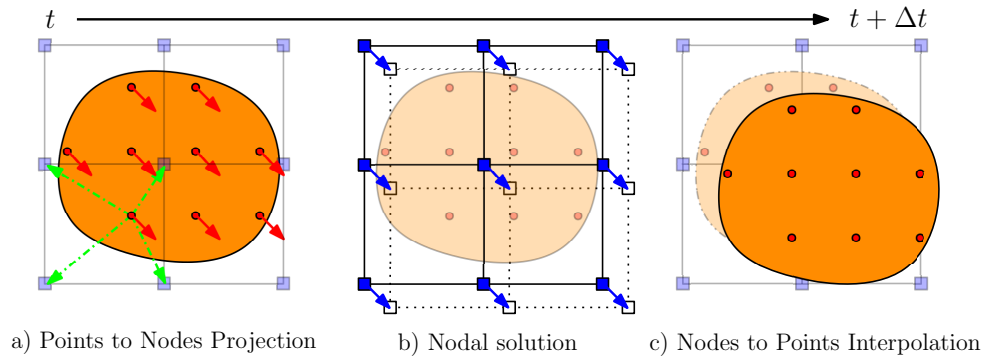


Figure 1: Typical calculation cycle of a MPM solver for a homogeneous velocity field, inspired by Dunatunga and Kamrin (2017). a) The continuum (orange) is discretized into a set of Lagrangian material points (red dots), at which state variables or properties (e.g., mass, stress, and velocity) are defined. The latter are mapped to an Eulerian finite element mesh made of nodes (blue square). b) Momentum equations are solved at the nodes and, the solution is explicitly advanced forward in time. c) The nodal solutions are interpolated back to the material points and, their properties are updated.

Comment # 9 The list of the three steps of a typical MPM cycle at the beginning of Section 3.1 seems misplaced and is somewhat repetitive of the description of MPM in the previous sections. I suspect this list should link with Fig. 1 and may be more appropriately located within Section 2.

Reply # 9 We agree with the Referee; this list is misplaced. Consequently, we moved it in the section "2. Overview of the Material Point Method (MPM)" within the subsection "2.1 A Material Point Method implementation" and, we directly refer to this list with Fig. 1.

Change # 9 See Change # 8

Comment # 10 Fig 2. In the caption, GIMP should be changed to GIMPM to match the rest of the paper. The authors have already fixed the error in Fig. 2b regarding which nodes are associated with the GIMPM domain.

Reply # 10 Right, we have made the change in the revised paper.

Change # 10 -

Comment # 11 Line 39: which numerical considerations from MILAMIN are used? This is not specifically addressed.

Reply # 11 Due to the comment of the first referee concerning the lack of focus in the introduction section, we partially have rewritten it. We now specify in the section "1. Introduction" the considerations we selected (from MILAMIN but also from the works of Birds et al, 2017 and OSullivan et al, 2019), which are the use of the function `accumarray()` and vectorisation activities mainly to reduce the number of BLAS calls.

Change # 11 (L64-70) These techniques include the use of `accumarray()`, optimal RAM-to-cache communication, minimum BLAS calls and the use of native MATLAB functions. We did not consider the blocking technique initially proposed by Dabrowski et al. (2008) since an explicit formulation in MPM excludes the global stiffness matrix assembly procedure. The performance gain mainly comes from the vectorisation of the algorithm, whereas blocking has a less significant impact over the performance gain, as stated by Bird et al. (2017).

Comment # 12 several citations are missing parentheses (e.g. lines 52 and 84).

Reply # 12 We have fixed these numerous citation problems in the revised paper.

Change # 12 -

References

- Acosta, J. L. G., Vardon, P. J., Remmerswaal, G., and Hicks, M. A.: An investigation of stress inaccuracies and proposed solution in the material point method, *Computational Mechanics*, 65, 555–581, 2020.
- Anderson Jr, C. E.: An overview of the theory of hydrocodes, *International journal of impact engineering*, 5, 33–59, 1987.
- Bandara, S., Ferrari, A., and Laloui, L.: Modelling landslides in unsaturated slopes subjected to rainfall infiltration using material point method, *International Journal for Numerical and Analytical Methods in Geomechanics*, 40, 1358–1380, 2016.
- Bardenhagen, S. G. and Kober, E. M.: The generalized interpolation material point method, *Computer Modeling in Engineering and Sciences*, 5, 477–496, 2004.
- Beuth, L., Benz, T., Vermeer, P. A., and Wieckowski, Z.: Large deformation analysis using a quasi-static material point method, *Journal of Theoretical and Applied Mechanics*, 38, 45–60, 2008.
- Bird, R. E., Coombs, W. M., and Giani, S.: Fast native-MATLAB stiffness assembly for SIPG linear elasticity, *Computers & Mathematics with Applications*, 74, 3209–3230, 2017.
- Charlton, T., Coombs, W., and Augarde, C.: iGIMP: An implicit generalised interpolation material point method for large deformations, *Computers & Structures*, 190, 108–125, 2017.
- Coombs, W. M. and Augarde, C. E.: AMPLE: A Material Point Learning Environment, *Advances in Engineering Software*, 139, 102 748, 2020.
- Coombs, W. M., Charlton, T. J., Cortis, M., and Augarde, C. E.: Overcoming volumetric locking in material point methods, *Computer Methods in Applied Mechanics and Engineering*, 333, 1–21, 2018.
- Coombs, W. M., Augarde, C. E., Brennan, A. J., Brown, M. J., Charlton, T. J., Knappett, J. A., Motlagh, Y. G., and Wang, L.: On Lagrangian mechanics and the implicit material point method for large deformation elasto-plasticity, *Computer Methods in Applied Mechanics and Engineering*, 358, 112 622, 2020.
- Cortis, M., Coombs, W., Augarde, C., Brown, M., Brennan, A., and Robinson, S.: Imposition of essential boundary conditions in the material point method, *International Journal for Numerical Methods in Engineering*, 113, 130–152, 2018.
- Dabrowski, M., Krotkiewski, M., and Schmid, D.: MILAMIN: MATLAB-based finite element method solver for large problems, *Geochemistry, Geophysics, Geosystems*, 9, 2008.
- Davis, T. A.: Suite Sparse, URL <https://people.engr.tamu.edu/davis/research.html>, 2013.
- de Souza Neto, E. A., Peric, D., and Owen, D. R.: *Computational methods for plasticity: theory and applications*, John Wiley & Sons, 2011.
- de Vaucorbeil, A., Nguyen, V., and Hutchinson, C.: A Total-Lagrangian Material Point Method for solid mechanics problems involving large deformations, 2020.
- Dunatunga, S. and Kamrin, K.: Continuum modeling of projectile impact and penetration in dry granular media, *Journal of the Mechanics and Physics of Solids*, 100, 45–60, 2017.
- Gaume, J., Gast, T., Teran, J., van Herwijnen, A., and Jiang, C.: Dynamic anticrack propagation in snow, *Nature communications*, 9, 1–10, 2018.
- Guilkey, J. E. and Weiss, J. A.: Implicit time integration for the material point method: Quantitative and algorithmic comparisons with the finite element method, *International Journal for Numerical Methods in Engineering*, 57, 1323–1338, 2003.

- Huang, P., Li, S.-l., Guo, H., and Hao, Z.-m.: Large deformation failure analysis of the soil slope based on the material point method, *computational Geosciences*, 19, 951–963, 2015.
- Iaconeta, I., Larese, A., Rossi, R., and Guo, Z.: Comparison of a material point method and a galerkin meshfree method for the simulation of cohesive-frictional materials, *Materials*, 10, 1150, 2017.
- Moler, C.: MATLAB Incorporates LAPACK, URL <https://ch.mathworks.com/de/company/newsletters/articles/matlab-2000>, 2000.
- Ni, R. and Zhang, X.: A precise critical time step formula for the explicit material point method, *International Journal for Numerical Methods in Engineering*, 121, 4989–5016, 2020.
- OSullivan, S., Bird, R. E., Coombs, W. M., and Giani, S.: Rapid non-linear finite element analysis of continuous and discontinuous galerkin methods in matlab, *Computers & Mathematics with Applications*, 78, 3007–3026, 2019.
- Sadeghirad, A., Brannon, R. M., and Burghardt, J.: A convected particle domain interpolation technique to extend applicability of the material point method for problems involving massive deformations, *International Journal for numerical methods in Engineering*, 86, 1435–1456, 2011.
- Sadeghirad, A., Brannon, R., and Guilkey, J.: Second-order convected particle domain interpolation (CPDI2) with enrichment for weak discontinuities at material interfaces, *International Journal for numerical methods in Engineering*, 95, 928–952, 2013.
- Simpson, G.: Practical finite element modeling in earth science using matlab, Wiley Online Library, 2017.
- Sinaie, S., Nguyen, V. P., Nguyen, C. T., and Bordas, S.: Programming the material point method in Julia, *Advances in Engineering Software*, 105, 17–29, 2017.
- Vermeer, P. A. and De Borst, R.: Non-associated plasticity for soils, concrete and rock, *HERON*, 29 (3), 1984, 1984.
- Wallstedt, P. C. and Guilkey, J.: An evaluation of explicit time integration schemes for use with the generalized interpolation material point method, *Journal of Computational Physics*, 227, 9628–9642, 2008.
- Wang, B., Hicks, M., and Vardon, P.: Slope failure analysis using the random material point method, *Géotechnique Letters*, 6, 113–118, 2016a.
- Wang, B., Vardon, P., and Hicks, M.: Investigation of retrogressive and progressive slope failure mechanisms using the material point method, *Computers and Geotechnics*, 78, 88–98, 2016b.
- Wang, B., Vardon, P. J., Hicks, M. A., and Chen, Z.: Development of an implicit material point method for geotechnical applications, *Computers and Geotechnics*, 71, 159–167, 2016c.
- Wang, L., Coombs, W. M., Augarde, C. E., Cortis, M., Charlton, T., Brown, M., Knappett, J., Brennan, A., Davidson, C., Richards, D., et al.: On the use of domain-based material point methods for problems involving large distortion, *Computer Methods in Applied Mechanics and Engineering*, 355, 1003–1025, 2019.
- Zhang, X., Chen, Z., and Liu, Y.: The material point method: a continuum-based particle method for extreme loading cases, Academic Press, 2016.

Fast and efficient MATLAB-based MPM solver (fMPMM-solver v1.0.1)

Emmanuel Wyser¹, Yury Alkhimenkov^{1,2,3}, Michel Jaboyedoff^{1,2}, and Yury Y. Podladchikov^{1,2,3}

¹Institute of Earth Sciences, University of Lausanne, 1015 Lausanne, Switzerland

²Swiss Geocomputing Centre, University of Lausanne, 1015 Lausanne, Switzerland

³Department of Mechanics and Mathematics, Moscow State University, Moscow, Russia

Correspondence: Emmanuel Wyser (manuwyser@gmail.com)

Abstract. ~~In this contribution, we~~ We present an efficient MATLAB-based implementation of the material point method (MPM) and its most recent variants.

MPM has gained popularity over the last decade, especially for problems in solid mechanics in which large deformations are involved, i.e., cantilever beam problems, granular collapses, and even large-scale snow avalanches. Although its numerical accuracy is lower than that of the widely accepted finite element method (FEM), MPM has been proven useful in overcoming some of the limitations of FEM, such as excessive mesh distortions.

We demonstrate that MATLAB is an efficient high-level language for MPM implementations that solve elasto-dynamic and elasto-plastic problems, ~~such as the cantilever beam and granular collapses,~~ We accelerate the MATLAB-based implementation of MPM method by using the numerical techniques recently developed for FEM optimization in MATLAB. These techniques include vectorisation, the usage of native MATLAB functions, the maintenance of optimal RAM-to-cache communication, and others. We validate our in-house code with classical MPM benchmarks including i) the elastic collapse under self-weight of a column, ii) the elastic cantilever beam problem, and iii) existing experimental and numerical results, i.e., granular collapses and slumping mechanics respectively. We report a ~~computational efficiency factor of 20 for a vectorized performance gain by a factor of 28 for a vectorised~~ code compared to a classical iterative version. ~~In addition, the numerical efficiency~~ The computational performance of the solver ~~surpassed is at least 2.8 times greater than~~ those of previously reported MPM implementations in Julia, ~~and minima 2.5 times faster~~ under a similar computational architecture.

1 Introduction

The material point method (MPM), developed in the 1990s (~~Sulsky et al. (1994)~~ (Sulsky et al., 1994)), is an extension of a particle-in-cell (PIC) method to solve solid mechanics problems involving massive deformations. It is an alternative to Lagrangian approaches (updated Lagrangian finite element method) that is well suited to problems with large deformations involved in geomechanics, granular mechanics or even snow avalanche mechanics. ~~Wang et al. (2016c); Vardon et al. (2017); Vardon et al. (2017); Wang et al. (2016c)~~ investigated elasto-plastic problems of strain localization of slumping processes relying on an explicit or implicit MPM formulation. Similarly, ~~Bandara et al. (2016); Bandara and Soga (2015)~~ Bandara et al. (2016); Bandara proposed a poro-elasto-plastic MPM formulation to study levee failures induced by pore pressure increases. Additionally,

25 ~~Dunatunga and Kamrin (2017, 2015); Więckowski (2004); Bardenhagen et al. (2000)~~ Baumgarten and Kamrin (2019); Dunatunga and Ka
proposed a general numerical framework of granular mechanics, i.e., silo discharge or granular collapses. More recently,
~~Gaume et al. (2018)~~ Gaume et al. (2019, 2018) proposed a unified numerical model in the finite deformation framework to
study the whole process, i.e., from failure to propagation, of slab avalanche releases.

The core idea of MPM is to discretize a continuum with material points carrying state variables (e.g., mass, stress, and
30 velocity). The latter are mapped (accumulated) to the nodes of a regular or irregular background FE mesh, on which an
Eulerian solution to the momentum balance equation is explicitly advanced forward in time.

Nodal solutions are then mapped back to the material points, and the mesh can be discarded. The mapping from material
points to nodes is ensured using the standard FE hat function that spans over an entire element (~~Bardenhagen and Kober (2004)~~
)(Bardenhagen and Kober, 2004). This avoids a common flaw of FEM, which is an excessive mesh distortion. We will refer to
35 this first variant as the standard material point method (sMPM).

MATLAB[®] allows a rapid code prototyping but, at the expense of significantly lower computational ~~performance than C~~
~~or C++~~. However, ~~Sinaie et al. (2017) recently demonstrated that an MPM implementation in Julia offers significantly higher~~
~~performances when compared to a similar implementation in MATLAB~~ performances than compiled language. An efficient
MATLAB implementation of FEM called MILAMIN (Million a Minute) was proposed by Dabrowski et al. (2008) that was ca-
40 pable of solving two-dimensional linear problems with one million unknowns in one minute on a modern computer with a rea-
sonable architecture. The efficiency of the algorithm lies on a combined use of vectorised calculations with a technique called
blocking. MATLAB uses the Linear Algebra PACKages (LAPACK), written in Fortran, to perform mathematical operations by
calling Basic Linear Algebra Subroutines (BLAS, Moler 2000). The latter results in an overhead each time a BLAS call is made.
Hence, mathematical operations over a large number of small matrices should be avoided and, operations on fewer and larger
45 matrices preferred. This is a typical bottleneck in FEM when local stiffness matrices are assembled during the integration
point loop within the global stiffness matrix. Dabrowski et al. (2008) proposed an algorithm, in which a loop reordering is
combined with operations on blocks of elements to address this bottleneck. However, data required for a calculation within a
block should entirely resides in the CPUs cache. Otherwise, an additional time is spent on the RAM-to-cache communication
and the performance decreases. Therefore, an optimal block size exists and, is solely defined by the CPU architecture. This
50 technique of vectorisation combined with blocking significantly increases the performance.

More recently, Bird et al. (2017) extended the vectorised and blocked algorithm presented by Dabrowski et al. (2008) to the
calculation of the global stiffness matrix for Discontinuous Galerkin FEM considering linear elastic problems using only native
MATLAB functions. Indeed, the optimisation strategy chosen by Dabrowski et al. (2008) also relied on non-native MATLAB
functions, e.g., `sparse2` of the SuiteSparse package (Davis, 2013). In particular, Bird et al. (2017) showed the importance
55 of storing vectors in a column-major form during calculation. Mathematical operations are performed in MATLAB by calling
LAPACK, written in FORTRAN, in which arrays are stored in column-major order form. Hence, element-wise multiplication
of arrays in column-major form is significantly faster and thus, vectors in column-major form are recommended, whenever
possible. Bird et al. (2017) concluded that vectorisation alone results in a performance increase between 13.7 and 23 times,
while blocking only improved vectorisation by an additional 1.8 times. O'Sullivan et al. (2019) recently extended the works

60 of Bird et al. (2017); Dabrowski et al. (2008) to optimised elasto-plastic codes for Continuous Galerkin (CG) or Discontinuous Galerkin (DG) methods. In particular, they proposed an efficient native MATLAB function, i.e., `accumarray()`, to efficiently assemble the internal force vector. Such function constructs an array by accumulation. More generally, O’Sullivan et al. (2019) reported a performance gain of x25.7 when using an optimised CG code instead of an equivalent non-optimised code.

Since MPM and FEM share common grounds, we aim at increasing the performances of MATLAB up to what was reported by Sinaie et al. (2017), ~~combining~~ using Julia language environment. In principal, Julia is significantly faster than MATLAB for a MPM implementation. We combine the most recent and accurate versions of MPM: the explicit ~~GIMPM~~ (generalized interpolation material point method, ~~Bardenhagen and Kober (2004)~~ (GIMPM, Bardenhagen and Kober 2004) and the explicit convected particle domain interpolation with second-order quadrilateral domains (CPDI2q, ~~Sadeghirad et al. (2013, 2011)~~ and CPDI, Sadeghirad et al. 2013, 2011) variants with some of the numerical ~~considerations from the FEM solver MILAMIN~~ techniques developed during the last decade of FEM optimisation in MATLAB. These techniques include the use of `accumarray()`, optimal RAM-to-cache communication, minimum BLAS calls and the use of native MATLAB functions. We did not consider the blocking technique initially proposed by Dabrowski et al. (2008) since an explicit formulation in MPM excludes the global stiffness matrix assembly procedure. The performance gain mainly comes from the vectorisation of the algorithm, whereas blocking has a less significant impact over the performance gain, as stated by Bird et al. (2017). The vectorisation of MATLAB functions is also crucial for a straight transpose of the solver to a more efficient language, such as the C-CUDA language, which allows the parallel execution of computational kernels of graphics processing units (GPUs).

In this ~~manuscript~~ contribution, we present an implementation of an efficiently ~~vectorized~~ vectorised explicit MPM solver (fMPMM-solver, which v1.0.1 is available for download from Bitbucket at: <https://bitbucket.org/ewyser/fmpmm-solver/src/master/>), taking advantage of ~~vectorization~~ vectorisation capabilities of MATLAB[®], i.e., ~~extensive use of built-in functions~~. We ~~extensively use native functions of MATLAB[®]~~ such as `repmat()`, `reshape()`, `sum()`, ~~`sparse()`~~ or `accumarray()`. We ~~compare our results with i) validate our in-house code with~~ classical MPM benchmarks, i.e., ~~including i) the elastic collapse under self-weight, and ii) validate our in-house code with of a column, ii) the elastic cantilever beam problem, and iii) existing experimental results, i.e., granular collapses~~. We ~~conclude by showcasing examples of applications to landslide mechanics and slumping mechanics~~. We demonstrate the computational efficiency of a vectorised implementation over an iterative one for the case of an elasto-plastic collapse of a column. We compare the performances of Julia and MATLAB language environments for the collision of two elastic discs problem.

2 Overview of the Material Point Method (MPM)

2.1 A Material Point Method implementation

The material point method (MPM), originally proposed by Sulsky et al. (1995, 1994) in an explicit ~~format~~ formulation, is an extension of the particle-in-cell (PIC) method.

The key idea is to solve the weak form of the momentum balance equation on ~~an~~ a FE mesh while state variables (e.g., stress, velocity or mass) are stored at Lagrangian points discretizing the continuum, i.e., the material points, which can move

according to the deformation of the grid ~~Dunatunga and Kamrin (2017)~~(Dunatunga and Kamrin, 2017). MPM could be regarded as a finite element solver in which integration points (material points) are allowed to move ~~(Guilkey and Weiss (2003))~~ and are thus not always located at the Gauss-Legendre location within an element, resulting in higher quadrature errors and poorer integration estimates, especially when using low-order basis functions ~~Steffen et al. (2008a); ?~~ ~~(Steffen et al., 2008a, b).~~

A typical calculation cycle (see Fig. 1) consists of the three following steps (Wang et al., 2016a):

1. A Mapping phase, during which properties of the material point (mass, momentum or stress) are mapped to the nodes.
2. An updated-Lagrangian FEM (UL-FEM) phase, during which the momentum equations are solved on the nodes of the background mesh and, the solution is explicitly advanced forward in time.
3. A Convection phase, during which i) the nodal solutions are interpolated back to the material points, and ii) the properties of the material point are updated.

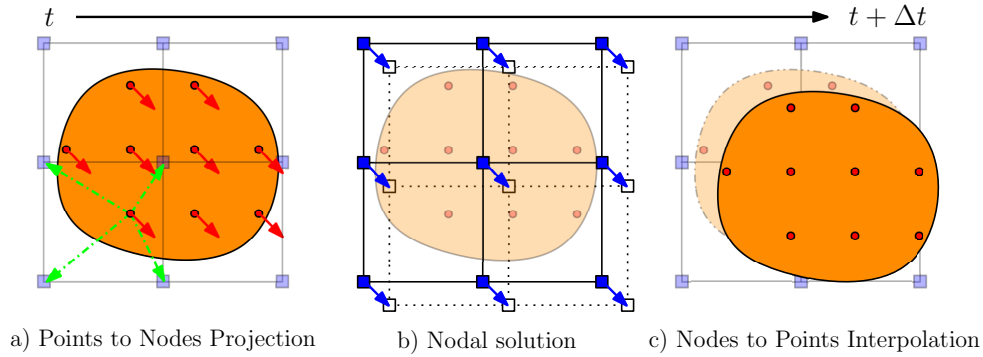


Figure 1. Typical calculation cycle of an MPM solver for a homogeneous velocity field, inspired by Dunatunga and Kamrin (2017). a) The continuum (orange) is discretized into a set of Lagrangian material points (red dots), at which state variables or properties (e.g., mass, stress, and velocity) are defined. The latter are mapped to an Eulerian finite element mesh made of nodes (blue square). b) Momentum equations are solved at the nodes and, the solution is explicitly advanced forward in time. c) The nodal solutions are interpolated back to the material points and, their properties are updated.

Since the 1990's, several variants were introduced to resolve a number of numerical issues. The generalized interpolation material point method (GIMPM) was first presented by Bardenhagen and Kober (2004)and-. They proposed a generalization of the basis and gradient functions that were convoluted with a characteristic domain function of the material point. A major flaw in sMPM is the lack of continuity of the gradient basis function, resulting in spurious oscillations of internal forces as soon as a material point crosses an element boundary while entering into its neighbour. This is referred to as cell-crossing instabilities due to the C_0 continuity of the gradient basis functions ~~,and it used in sMPM. Such issue~~ is minimized by the GIMPM variant ~~-~~ This variant allows the material point's domain to deform (cpGIMPM) or not (uGIMPM) according to its deformation gradient tensor (see Coombs et al. (2020)). Hence, (Acosta et al., 2020).

GIMP is categorized as a domain-based material point method, unlike the later development of the B-spline material point method (BSMPM, [see Gaume et al. \(2018\); ?; Steffen et al. \(2008a\)](#), e.g. [de Koster et al. 2020; Gan et al. 2018; Gaume et al. 2018; Stomak](#)) which cures cell-crossing instabilities using B-spline functions as basis functions. Whereas in sMPM only nodes belonging to an element contribute to a given material point, GIMP requires an extended nodal connectivity, i.e., the nodes of the element enclosing the material point and the nodes belonging to the adjacent elements (see Fig. 2). Last More recently, the convected particle domain interpolation [proposed by Sadeghirad et al. \(2013, 2011\)](#) accounts for the deformation and the rotation of the material point's domain, the latter being considered either as a deforming parallelogram (CPDI) or as a deforming quadrilateral ((CPDI and its most recent development CPDI2q). These variants require some additional considerations during the vectorization task [has been proposed by Sadeghirad et al. \(2013, 2011\)](#).

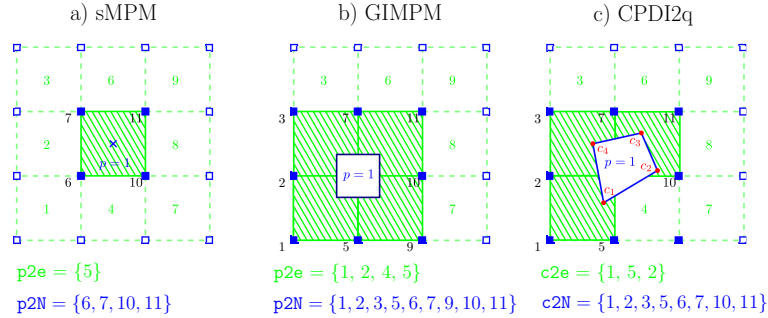


Figure 2. Nodal connectivities of a) standard MPM and, b) GIMP and c) CPDI2q variants. The material point's location is marked by the blue cross. Note that for sMPM (and similarly BSMPM) the particle domain does not exist, unlike for GIMP or CPDI2q (the blue square enclosing the material point). Nodes associated with the material point are denoted by filled blue squares, and the element number appears in green in the center of the element. For sMPM and GIMP, the connectivity array between the material point and the element is $p2e$ and, the array between the element-material point and its associated nodes is $e2N$ and $p2N$. For CPDI2q, the connectivity array between the corners (filled red circles) of the quadrilateral domain of the material point and its element is $c2e$ and, the array between the corners and their associated nodes is $p2N$ and $c2N$.

120

We choose the explicit GIMP variant with the modified update stress last scheme (MUSL, see Nairn (2003); Bardenhagen et al. (2000) for a detailed discussion), i.e., the stress of material point is updated after the nodal solutions are obtained. The updated momentum of the material point is then mapped back a second time to the nodes in order to obtain an updated nodal velocity, further used to calculate gradient derivative terms such as the strains or the deformation gradient of the material point. The explicit format formulation also implies the well-known restriction on the time step, which is limited by the Courant-Friedrich-Lewy (CFL) condition to ensure numerical stability. The domain update is based on the diagonal components of the stretch tensor of the material point (Charlton et al. (2017)), which ensures optimal convergence properties according to Coombs et al. (2020).

Additionally, we implemented a CPDI/CPDI2q version (in an explicit and quasi-static implicit format formulation) of the solver. However, in this paper, we do not present the theoretical background of the CPDI variant nor the implicit imple-

130

mentation of ~~an a~~ MPM-based solver, ~~and therefore~~. Therefore, interested readers are referred to the original contributions of Sadeghirad et al. (2013, 2011) and ~~Charlton et al. (2017); Iaconeta et al. (2017); Beuth et al. (2008); Guilkey and Weiss (2003)~~ Acosta et al. (2020); Charlton et al. (2017); Iaconeta et al. (2017); Beuth et al. (2008); Guilkey and Weiss (2003), respectively. Regarding the quasi-static implicit implementation, we strongly adapted our vectorisation strategy to some aspects of the numerical implementation proposed by Coombs and Augarde (2020) in the MATLAB code AMPLE v1.0. However, we did not consider blocking, because our main concern for performance is on the explicit implementation.

3 MATLAB-based MPM implementation

2.1 ~~Structure of the MPM solver~~The solver procedure is shown in Fig.3. ~~A typical MPM calculation cycle consists of the three following steps Wang et al. (2016a): A Mapping phase, during which properties of the Domain-based material point (mass, momentum or stress) are mapped to the nodes.~~ method variants

Domain-based material point method variants could be treated as two distinct groups:

- The material point's domain is a square for which the deformation is always aligned with the mesh axis, i.e., a non-deforming domain uGIMPM (Bardenhagen and Kober, 2004) or, a deforming domain cpGIMPM (Wallstedt and Guilkey, 2008), the latter being usually related to a measure of the deformation, e.g., the determinant of the deformation gradient.
 - ~~An Updated-Lagrangian FEM (UL-FEM) phase, during which the momentum equations are solved on the nodes and the solution is explicitly advanced forward in time.~~ The material point's domain is either a deforming parallelogram for which its dimensions are specified by two vectors, i.e., CPDI (Sadeghirad et al., 2011), or a deforming quadrilateral solely defined by its corners, i.e., CPDI2q (Sadeghirad et al., 2013). However, the deformation is not necessarily aligned with the mesh anymore.
- 150 We first focus on the different domain updating methods for GIMPM. Four domain updating methods exists: i) the domain is not updated, ii) the deformation of the domain is proportional to the determinant of the deformation gradient $\det(F_{ij})$ (Bardenhagen and Kober, 2004), iii) the domain lengths l_p are updated accordingly to the principal component of the deformation gradient F_{ij} (Sadeghirad et al., 2011) or, iv) are updated with the principal component of the stretch part of the deformation gradient U_{ij} (Charlton et al., 2017). Coombs et al. (2020) highlighted the suitability of generalised interpolation domain updating
- 155 methods accordingly to distinct deformation modes. Four different deformation modes were considered by Coombs et al. (2020) : simple stretch, hydrostatic compression/extension, simple shear and, pure rotation. Coombs et al. (2020) concluded the following:
- ~~A Convection phase, during which i) the nodal solutions are interpolated back to the material points.~~ Not updating the domain is not suitable for simple stretch and hydrostatic compression/extension.
 - A domain update based on $\det(F_{ij})$ will results in an artificial contraction/expansion of the domain for simple stretch.

- The domain will vanish with increasing rotation when using F_{ij} .
- The domain volume will change under isochoric deformation when using U_{ij} .

Consequently, Coombs et al. (2020) proposed a hybrid domain update inspired by CPDI2q approaches: the corners of the material point domain are updated accordingly to the nodal deformation but, the midpoints of the domain limits are used to update domain lengths l_p to maintain a rectangular domain. Even though Coombs et al. (2020) reported an excellent numerical stability, the drawback is to compute specific basis functions between nodes and material point's corners, which has an additional computational cost. Hence, we did not selected this approach in this contribution.

Regarding the recent CPDI/CPDI2q, Wang et al. (2019) investigated the numerical stability under stretch, shear and torsional deformation modes. CPDI2q was found to be erroneous in some case, especially when torsion mode is involved, due to distortion of the domain. In contrast, CPDI and even sMPM performed better in modelling torsional deformations. Even though CPDI2q can exactly represent the deformed domain (Sadeghirad et al., 2013), care must be taken when dealing with very large distortion, especially when the material has yielded, which is common in geotechnical engineering (Wang et al., 2019).

Consequently, the domain-based method as well as the domain updating method should be carefully chosen accordingly to the deformation mode expected for a given case. The latter will be always specify in the following and, the domain update method will be clearly stated.

3 MATLAB-based MPM implementation

3.1 Rate formulation and elasto-plasticity

The large deformation framework in a linear elastic continuum requires an appropriate stress-strain formulation. One approach is based on the finite deformation framework, which relies on a linear relationship between elastic logarithmic strains and Kirchhoff stresses (Coombs et al., 2020; Gaume et al., 2018; Charlton et al., 2017). In this study, we adopt another approach, namely, a rate dependent formulation using the Jaumann stress rate (e.g. Huang et al. 2015; Bandara et al. 2016; Wang et al. 2016c, b). This formulation provides an objective (invariant by rotation or frame-indifferent) stress rate measure (de Souza Neto et al., 2011) and is simple to implement. The Jaumann rate of the Cauchy stress is defined as

$$\frac{\mathcal{D}\sigma_{ij}}{\mathcal{D}t} = \frac{1}{2} C_{ijkl} \left(\frac{\partial v_l}{\partial x_k} + \frac{\partial v_k}{\partial x_l} \right), \quad (1)$$

where C_{ijkl} is the fourth rank tangent stiffness tensor and v_k is the velocity. Thus, the Jaumann stress derivative can be written as

$$\frac{\mathcal{D}\sigma_{ij}}{\mathcal{D}t} = \frac{D\sigma_{ij}}{Dt} - \sigma_{ik}\omega_{jk} - \sigma_{jk}\omega_{ik}, \quad (2)$$

where $\omega_{ij} = (\partial_i v_j - \partial_j v_i)/2$ is the vorticity tensor and $D\sigma_{ij}/Dt$ denotes the material derivative

$$\frac{D\sigma_{ij}}{Dt} = \frac{\partial \sigma_{ij}}{\partial t} + v_k \frac{\partial \sigma_{ij}}{\partial x_k}. \quad (3)$$

190 Plastic deformation is modelled with a pressure dependent Mohr-Coulomb law with non-associated plastic flow, i.e., both the dilatancy angle ψ and the volumetric plastic strain ϵ_v^p are null (Vermeer and De Borst, 1984). We have adopted the approach of Simpson (2017) for a two dimensional linear elastic, perfectly plastic (elasto-plasticity) continuum because of its simplicity and its ease of implementation. The yield function is defined as

$$f = \tau + \sigma \sin \phi - c \cos \phi, \quad (4)$$

195 where c is the cohesion and ϕ the angle of internal friction,

$$\sigma = (\sigma_{xx} + \sigma_{yy})/2, \quad (5)$$

and ii) the properties of the material point are updated.

$$\tau = \sqrt{(\sigma_{xx} - \sigma_{yy})^2/4 + \sigma_{xy}^2}. \quad (6)$$

200 The elastic state is defined when $f < 0$. However when $f > 0$, plastic state is declared and stresses must be corrected (or scaled) to satisfy the condition $f = 0$, since $f > 0$ is an inadmissible state. Simpson (2017) proposed the following simple algorithm to return stresses to the yield surface,

$$\sigma_{xx}^* = \sigma + (\sigma_{xx} - \sigma_{yy})\beta/2, \quad (7)$$

$$\sigma_{yy}^* = \sigma - (\sigma_{xx} - \sigma_{yy})\beta/2, \quad (8)$$

205

$$\sigma_{xy}^* = \sigma_{xy}\beta, \quad (9)$$

where $\beta = (|c \cos \phi - \sigma \sin \phi|)/\tau$, and σ_{xx}^* , σ_{yy}^* and σ_{xy}^* are the corrected stresses, i.e., $f = 0$.

A similar approach is used to return stresses when considering a non-associated Drucker-Prager plasticity (see Huang et al. (2015) for a detailed description of the procedure). In addition, their approach allows also to model associated plastic flows, i.e., $\psi > 0$ and $\epsilon_v^p \neq 0$.

210

3.2 Structure of the MPM solver

The solver procedure is shown in Fig. 3. In the `main.m` script, both functions `meSetup.m` and `mpSetup.m`, respectively, define the geometry and related quantities, particularly such as the nodal connectivity array, i.e. (or element topology) array, e.g., the `e2N` array (Simpson (2017)). The latter stores the nodes associated with a given element. As such, a material point p located in an element e can immediately identify which nodes \mathcal{N}_n it is associated with.

215

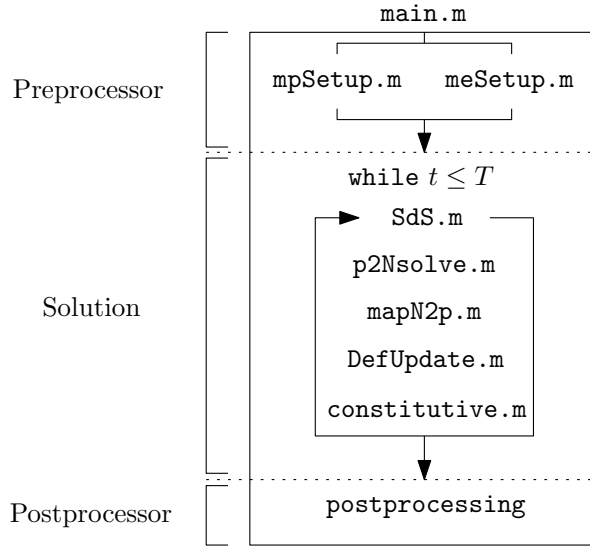


Figure 3. Workflow of the explicit GIMPM solver and the calls to functions within a calculation cycle. The role of each function is described in the text.

After initialization, a while loop solves the elasto-dynamic (or elasto-plastic) problem until a time criterion T is reached. This time criterion could be restricted to the time needed for the system to reach an equilibrium, or if the global kinetic energy of the system has reached a threshold.

At the beginning of each cycle, a connectivity array $p2e$ between the material points and their respective element (a material point can only reside in a single element) is ~~created~~constructed. Since i) the nodes associated with the elements and ii) the elements enclosing the material points are known, it is possible to obtain the connectivity array $p2N$ between the material points and their associated nodes, e.g., $p2N = e2N(p2e, :)$ in a MATLAB syntax (see Fig. 2 for an example of these connectivity arrays). This array is of dimension ~~(n_p, n_{Ne})~~ (n_p, n_n) , with n_p the total number of material points, ~~n_{Ne}~~ n_n the total number of nodes associated with an element (16 in two-dimensional problems) and $n_{i,j}$ the node number where i corresponds to the material point and j corresponds to its j -th associated nodes, which results in the following:

$$p2N = \begin{pmatrix} n_{1,1} & \cdots & n_{1,n_n} \\ \vdots & \ddots & \vdots \\ n_{n_p,1} & \cdots & n_{n_p,n_n} \end{pmatrix}. \quad (10)$$

The following functions are called successively during one calculation cycle:

1. `SdS.m` calculates the basis functions~~and the gradient of the basis functions and~~, derivatives and, assembles the strain-displacement matrix for each material points.

- 230 2. `p2Nsolve.m` projects the quantities of the material point (e.g., mass and momentum) to the associated nodes, solves the equations of motion and sets ~~Dirichlet~~-boundary conditions.
3. `mapN2p.m` interpolates nodal solutions (acceleration and velocity) to the material points with a double mapping procedure (see Zhang et al. (2016) or Nairn (2003) for a clear discussion of USF, USL and MUSL algorithms).
- 235 4. `DefUpdate.m` updates incremental strains and deformation-related quantities (e.g., the volume of the material point or the domain half-length) at the level of the material point based on the remapping of the updated material point momentum.
5. `constitutive.m` calls two functions to solve for the constitutive elasto-plastic relation, i.e.,
- (a) `elastic.m`, which predicts an incremental objective ~~stress-rate (the Jaumann stress-rate is selected for its ease of implementation and its acknowledged accuracy) considering stress assuming~~ a purely elastic step, further corrected
- 240 by
- (b) `plastic.m`, which corrects the trial stress by a plastic correction if the material has yielded.

When a time criterion is met, the calculation cycle stops and further post-processing tasks (visualization, data exportation) can be performed.

The numerical simulations are conducted using MATLAB[®] R2018a within a Windows 7 64-bit environment on an Intel
 245 Core i7-4790 (4th generation CPU with 4 physical cores of base frequency at 3.60 GHz up to a maximum turbo frequency of 4.00 GHz) with ~~8-MB~~ 4 × 256 kB L2 cache and 16 GB DDR3 RAM (clock speed 800 MHz).

3.3 ~~Vectorization~~Vectorisation

3.3.1 Basis ~~Functions~~functions and derivatives

The GIMPM basis function (~~Coombs et al. (2018); Steffen et al. (2008a); Bardenhagen and Kober (2004)~~) (Coombs et al., 2018; Steffen et al.)
 250 results from the convolution of a characteristic particle function χ_p (i.e., the material point spatial extent or domain) with the standard basis function ~~$N_T(x_p)$~~ $N_n(x)$ of the mesh, which results in:

$$S_{\underline{In}}(x_p) = \begin{cases} 1 - (4x^2 + l_p^2)/(4hl_p) & \text{if } |x| < l_p/2 \\ 1 - |x|/h & \text{if } l_p/2 \leq |x| < h - l_p/2 \\ (h + l_p/2 - |x|)^2/(2hl_p) & \text{if } h - l_p/2 \leq |x| < h + l_p/2 \\ 0 & \text{otherwise,} \end{cases} \quad (11)$$

with l_p the length of the material point domain, h the mesh spacing, ~~$x = x_p - x_T$~~ $x = x_p - x_n$ where x_p is the coordinate of a material point and ~~x_T~~ x_n the coordinate of its associated node ~~T~~ n . The basis function of a node ~~T~~ n with its material point p is

255 constructed for a two-dimensional model, as follows:

$$S_{\underline{In}}(\mathbf{x}_p) = S_{\underline{In}}(x_p)S_{\underline{In}}(y_p), \quad (12)$$

for which the derivative is defined as:

$$\nabla S_{\underline{In}}(\mathbf{x}_p) = (\partial_x S_{\underline{In}}(x_p)S_{\underline{In}}(y_p), S_{\underline{In}}(x_p)\partial_y S_{\underline{In}}(y_p)). \quad (13)$$

260 Within the GIMP variant, uGIMP (undeformed GIMP) and cpGIMP (contiguous particle GIMP) can be chosen to update the material point domain length l_p^0 , i.e., $l_p = l_p^0$ for the undeformed GIMP, $l_{i,p} = \det(F_{jk})l_{i,p}^0$ or $l_{i,p} = F_{ii}l_{i,p}^0$ where F_{ii} is the diagonal component of the deformation gradient for the cpGIMP. However, Charlton et al. (2017) recommend using the diagonal components $U_{ii} = (F_{kj}F_{ki})^{0.5}$ of the stretch part of the deformation gradient instead of the deformation gradient. Hence, the variant we use relies either on the determinant or on the stretch part of the deformation gradient.

265 Similar to the FEM, the strain-displacement matrix \mathbf{B} consists of the derivatives of the basis function and is assigned to each material point, which results in the following:

$$\mathbf{B}(\mathbf{x}_p) = \begin{pmatrix} \partial_x S_1 & 0 & \cdots & \partial_x S_{n_n} & 0 \\ 0 & \partial_y S_1 & \cdots & 0 & \partial_y S_{n_n} \\ \partial_y S_1 & \partial_x S_1 & \cdots & \partial_y S_{n_n} & \partial_x S_{n_n} \end{pmatrix}, \quad (14)$$

where $n_{Ne}n_n$ is the total number of associated nodes to an element e , in which a material point p resides.

The algorithm outlined in Code Fragment 1 Fig. 4 (the function [mpD] = SdS(meD, mpD, p2N) called at the beginning of each cycle, see Fig. 4) represents the ~~vectorized~~ vectorised solution of the computation of basis functions and their derivatives ~~in just one time step, which avoids any for-loop requirement.~~

Table B1 lists the variables used in Code fragments 1 & 2 (Figs. 4 & 5).

Coordinates of the material points $\text{mpD} \cdot x (:, 1:2)$ are first replicated and then subtracted by their associated nodes coordinates, e.g., $\text{meD} \cdot x (\text{p2N})$ ~~or and~~ $\text{meD} \cdot y (\text{p2N})$ respectively (Lines 3 or 4 in 5 in Fig. 4). This yields the array D with the same dimension of p2N. This array of distance between the points and their associated nodes is sent as an input to the ~~local~~ nested function $[N, dN] = \text{NdN}(D, h, l_p)$, which computes 1D basis ~~functions and derivatives through matrix piecewise function and its derivative through matrix element-wise~~ operations (operator $\cdot *$) (either in Line 4 for x coordinates or Line 6 for y coordinates in Fig. 4). ~~Note that the use of one single array D avoids a redundant usage of memory.~~

Given the piecewise piece-wise Eq. 11, three logical arrays (c1, c2 and c3) are defined (Lines 28-30 21-24 in Fig. 4), whose elements are either 1 (the condition is true) or 0 (the condition is false). Three arrays of basis functions are calculated (N1, N2 and N3, Lines 32-34 26-28) according to Eq. 12. The array of basis functions N is obtained through a summation of the elementwise element-wise multiplications of these temporary arrays with their corresponding logical arrays (Line 35-29 in Fig. 4). The same holds true for the calculation of the gradient basis function (Lines 37-40 31-34 in Fig. 4). ~~Furthermore,~~ It is faster to use logical arrays as multipliers of precomputed basis function arrays rather than using these in a conditional indexing statement, e.g., $N(c2==1) = 1 - \text{abs}(dX(c2==1)) \cdot h$. The performance gain is significant between the two ~~approaches~~, i.e., a-an intrinsic 30 % gain over ~~a-calculatione cycle.~~

Description of variables of the structure arrays for the mesh `meD` and the material point `mpD` used in Code Fragment 1 & 2 shown in Figs. 4 & 5. `nDF` stores the local and global number of degrees of freedom, i.e., `nDF=nNe,nN*DoF`. The constant `nstr` is the number of stress components, according to the standard definition of the Cauchy stress tensor using the Voigt notation, e.g., $\sigma_p = (\sigma_{xx}, \sigma_{yy}, \sigma_{xy})$. `nNe` nodes per element (1) `nN` number of nodes (1) `DoF` degree of freedom (1) `nDF` number of DoF (1,2) `h` mesh spacing (1,DoF) \times node coordinates (nN,1) `y` node coordinates (nN,1) `m` node mass (nN,1) `p` node momentum (nDF(2),1) `f` node force (nDF(2),1) `n` number of points (1) `l` domain half-length (np,DoF) `V` volume (np,1) `m` mass (np,1) \times point coordinates (np,DoF) `p` momentum (np,DoF) `s` stress (np,nstr) `S` basis function (np,nNe) `dSx` derivative in x (np,nNe) `dSy` derivative in y (np,nNe) `B` B-matrix (nstr,nDF(1),np) the wall-clock time of the basis functions and derivatives calculation. We observe an invariance of such gain with respect to the initial number of material point per element or to the mesh resolution.

```

1 function [mpD] = SdS(meD,mpD,p2N)
2 % COMPUTE (X,Y)-BASIS FUNCTION
3 D = (repmat(mpD.x(:,1),1,meD.nNe) - meD.x(p2N)); %
4 [Sx,dSx] = NdN(D,meD.h(1),repmat(mpD.1(:,1),1,meD.nNe)); %
5 D = (repmat(mpD.x(:,2),1,meD.nNe) - meD.y(p2N)); %
6 [Sy,dSy] = NdN(D,meD.h(2),repmat(mpD.1(:,2),1,meD.nNe)); %
7 % CONVOLUTION OF BASIS FUNCTIONS
8 mpD.S = Sx.* Sy ; %
9 mpD.dSx = dSx.* Sy ; %
10 mpD.dSy = Sx.* dSy ; %
11 % B MATRIX ASSEMBLY
12 iDx = 1:meD.DoF:meD.nDoF(1)-1 ; %
13 iDy = iDx+1 ; %
14 mpD.B(1,iDx,:) = mpD.dSx' ; %
15 mpD.B(2,iDy,:) = mpD.dSy' ; %
16 mpD.B(3,iDx,:) = mpD.dSy' ; %
17 mpD.B(3,iDy,:) = mpD.dSx' ; %
18 end
19 function [N,dN]=NdN(dX,h,lp)
20 % COMPUTE BASIS FUNCTIONS
21 lp = 2*lp ; %
22 c1 = (abs(dX)<( 0.5*lp) ) ; %
23 c2 = ((abs(dX)>=( 0.5*lp)) & (abs(dX)<(h-0.5*lp))) ; %
24 c3 = ((abs(dX)>=(h-0.5*lp)) & (abs(dX)<(h+0.5*lp))) ; %
25 % BASIS FUNCTION
26 N1 = 1-((4*dX.^2+lp.^2)./(4*h.*lp)) ; %
27 N2 = 1-(abs(dX)./h) ; %
28 N3 = ((h+0.5*lp-abs(dX)).^2)./(2*h.*lp) ; %
29 N = c1.*N1+c2.*N2+c3.*N3 ; %
30 % BASIS FUNCTION GRADIENT
31 dN1= -(8*dX)./(4*h.*lp) ; %
32 dN2= sign(dX).*(-1/h) ; %
33 dN3=-sign(dX).*(h+0.5*lp-abs(dX))./(h*lp) ; %
34 dN = c1.*dN1+c2.*dN2+c3.*dN3 ; %
35 end

```

Figure 4. Code Fragment 1 shows the vectorized solution to the calculation of the basis functions and their gradients within the function `SdS.m`. Table B1 lists the variables used.

3.3.2 Integration of internal forces

Another computationally expensive operation for MATLAB[®] is the mapping (or accumulation) of the material point contributions to their associated nodes. It is performed by the function `p2Nsolve.m` in the workflow of the solver.

The standard calculations for the material point contributions to the lumped mass $\underline{m}_I \underline{m}_n$, the momentum $\underline{p}_I \underline{p}_n$, the external \underline{f}_I^e and internal \underline{f}_I^i forces are given by:

$$\underline{m}_I = \sum_{p \in I} S_{In}(x_p) m_p, \quad (15)$$

$$\underline{p}_I = \sum_{p \in I} S_{In}(x_p) m_p \underline{v}_p, \quad (16)$$

$$\underline{f}_I^e = \sum_{p \in I} S_{In}(x_p) m_p \underline{b}_p, \quad (17)$$

$$\underline{f}_I^i = \sum_{p \in I} v_p \underline{B}^T(x_p) \underline{\sigma}_p, \quad (18)$$

with m_p the material point mass, \underline{v}_p the material point velocity, \underline{b}_p the body force applied to the material point and $\underline{\sigma}_p$ the material point Cauchy stress tensor in the Voigt notation.

Once the mapping phase is achieved, the equations of motions are explicitly solved forward in time on the mesh. Nodal accelerations \underline{a}_n and velocities \underline{v}_n are given by:

$$\underline{a}_n^{t+\Delta t} = \underline{m}_n^{-1} (\underline{f}_n^e - \underline{f}_n^i), \quad (19)$$

$$\underline{v}_n^{t+\Delta t} = \underline{m}_n^{-1} \underline{p}_n + \Delta t \underline{a}_n^{t+\Delta t}. \quad (20)$$

Finally, boundary conditions are applied to the nodes that belong to the boundaries.

The ~~vectorized~~ vectorised solution comes from the use of the built-in function `accumarray()` of MATLAB[®] combined with `reshape()` and `repmat()`. ~~Similar to the function `sparse()`, `accumarray()` collects, in a vector \underline{e} , and accumulates, into a second vector \underline{e}' , all values in \underline{e} that have identical subscripts, whose values are contained in a vector \underline{s} . Such an operation corresponds to the summation operator in Eqs. 15-18.~~ The core of the vectorization is to use `p2N` as the a vector (i.e., flattening the array `p2N(:)` results in a row vector) of subscripts with `accumarray`, which accumulates material point contributions (e.g., mass or momentum) that share the same node.

In the function `p2Nsolve` (Code Fragment 2 shown in Fig. 5), the first step is to initialize nodal vectors (mass, momentum, forces, etc.) to zero (Lines 4-5 in Fig. 5). Then, temporary vectors (`m`, `p`, `f` and `fi`) of material point contributions (namely, mass, momentum, and external and internal forces) are generated (Lines 10-17 in Fig. 5). The accumulation (nodal summation) is performed (Lines 19-26 in Fig. 5) using either the flattened `p2n(:)` or `l2g(:)` (e.g., the global indices of nodes) as the vector of subscripts. Note that for the accumulation of material point contributions of internal forces, a short for-loop iterates over the associated node (e.g., from 1 to `meD.nNe`) of every material point to accumulate their respective contributions.

To calculate the temporary vector of internal forces (`fi` at Lines 15-17 in Fig. 5), the first step consists of the matrix multiplication of the strain-displacement matrix `mpD.B` with the material point stress vector `mpD.s`. The ~~vectorized~~ vectorised solution is given by i) ~~elementwise multiplications of a permutation~~ element-wise multiplications of `permute(mpD.B, 2-1-3)` (e.g., the transpose operator for multidimensional arrays) with a replication of the transposed stress vector `repmat(permute(reshape(mpD.s, 2-1), 1, mpD.n), 1, meD.nDfNDof(1), 1)`, whose result is then ii) summed by means of the built-in function `sum()` along the columns and, finally multiplied by a replicated transpose of the material point volume vector, e.g., `repmat(permute(V, 2-1)', meD.nDfNDof(1), 1)`.

```

1 function [meD] = p2Nsolve(meD,mpD,g,dt,l2g,p2N,bc)
2 %% INITIALIZATION
3 % NODAL VECTOR INITIALIZATION
4 meD.m(:) = 0.0 ; meD.mr(:) = 0.0 ; meD.f(:) = 0.0 ; meD.d(:) = 0.0 ;%
5 meD.a(:) = 0.0 ; meD.p(:) = 0.0 ; meD.v(:) = 0.0 ; meD.u(:) = 0.0 ;%
6 %% CONTRIBUTION TO NODES
7 % PREPROCESSING
8 m = reshape( mpD.S.*repmat(mpD.m,1,meD.nNe) ,mpD.n*meD.nNe ,1) ;%
9 p = reshape([mpD.S.*repmat(mpD.p(:,1),1,meD.nNe);...
10             mpD.S.*repmat(mpD.p(:,2),1,meD.nNe)],mpD.n*meD.nDoF(1),1) ;%
11 f = reshape([mpD.S.*0.0 ;...
12             mpD.S.*repmat(mpD.m,1,meD.nNe).*-g ],mpD.n*meD.nDoF(1),1) ;%
13 fi= squeeze(sum(mpD.B.*repmat(reshape(mpD.s,size(mpD.s,1),1,mpD.n)...
14             ,1,meD.nDoF(1)),1)).*repmat(mpD.V',meD.nDoF(1),1) ;%
15 % CONTRIBUTION FROM p TO N
16 meD.m = accumarray(p2N(:,n),m,[meD.nN 1]) ;%
17 meD.p = accumarray(l2g(:,p),[meD.nDoF(2) 1]) ;%
18 meD.f = accumarray(l2g(:,f),[meD.nDoF(2) 1]) ;%
19 for n = 1:meD.nNe
20     l = [(meD.DoF*p2N(:,n)-1);(meD.DoF*p2N(:,n))] ;%
21     meD.f = meD.f - accumarray(l,[fi(n*meD.DoF-1,:);...
22                               fi(n*meD.DoF ,:)]',[meD.nDoF(2) 1]) ;%
23 end %
24 %% SOLVE EXPLICIT MOMENTUM BALANCE EQUATION
25 % UPDATE GLOBAL NODAL INFORMATIONS
26 iDx = 1:meD.DoF:meD.nDoF(2)-1 ;%
27 iDy = iDx+1 ;%
28 % COMPUTE GLOBAL NODAL FORCE
29 meD.d(iDx) = sqrt(meD.f(iDx).^2+meD.f(iDy).^2) ;%
30 meD.d(iDy) = meD.d(iDx) ;%
31 meD.f = meD.f - meD.vd*meD.d.*sign(meD.p) ;%
32 % UPDATE GLOBAL NODAL MOMENTUM
33 meD.p = meD.p + dt*meD.f ;%
34 % COMPUTE GLOBAL NODAL ACCELERATION AND VELOCITY
35 meD.mr = reshape(repmat(meD.m',meD.DoF,1),meD.nDoF(2),1) ;%
36 iD = meD.mr==0 ;%
37 meD.a = meD.f./meD.mr ;%
38 meD.v = meD.p./meD.mr ;%
39 meD.a(iD) = 0.0 ;%
40 meD.v(iD) = 0.0 ;%
41 % BOUNDARY CONDITIONS: FIX DIRICHLET BOUNDARY CONDITIONS
42 meD.a(bc.x(:,1))=bc.x(:,2) ;%
43 meD.a(bc.y(:,1))=bc.y(:,2) ;%
44 meD.v(bc.x(:,1))=bc.x(:,2) ;%
45 meD.v(bc.y(:,1))=bc.y(:,2) ;%
46 end

```

Figure 5. Code Fragment 2 shows the vectorized solution to the nodal projection of material point quantities (e.g., mass and momentum) within the local function `p2Nsolve.m`. The core of the vectorization process is the extensive use of the built-in function of MATLAB[®] `accumarray()`, for which we detail the main features in the text. [Table B1 lists the variables used.](#)

To illustrate the ~~efficiency of such a procedure~~ numerical efficiency of the vectorised multiplication between a matrix and a vector, we have developed an iterative and ~~vectorized~~ vectorised solution of $B(x_p)^T \sigma_p$ with an increasing n_p and ~~survey the computational time spent on solving the problem. We report again in computational time (close to an order of magnitude faster for one order of increase in magnitude of n_p for considering single (4 bytes) and double (8 bytes) arithmetic precision. The wall-clock time increases with n_p with a sharp transition for the vectorised solution around $n_p \approx 1000$, as showed in Fig 6a. The mathematical operation requires more memory than available in the vectorized solution) L2 cache (1024 kB under the CPU architecture used), which inhibits cache reuse (Dabrowski et al., 2008). A peak performance of at least 1000 Mflops, showed in Fig. 6b, is achieved when $n_p = 1327$ or $n_p = 2654$ for simple or double arithmetic precision respectively, i.e., it corresponds exactly to 1024 kB for both precisions. Beyond, the performance dramatically drops to approximately the half of the peak value. This drop is even more severe for a double arithmetic precision.~~

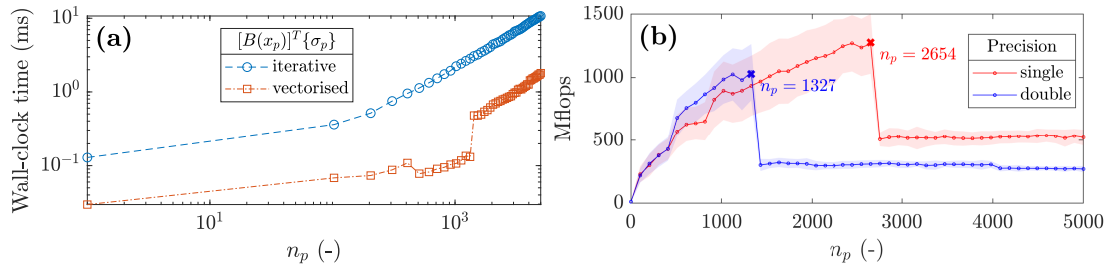


Figure 6. ~~Computational~~ a) Wall-clock time needed to solve for a matrix multiplication between a multidimensional array and a vector with an increasing number of the third dimension with a double arithmetic precision and, b) number of floating point operations per second (flops) for single and double arithmetic precisions. The continuous line represents the averages value whereas the shaded area denotes the standard deviation.

3.3.3 Update of material point properties

Finally, we propose a ~~vectorization~~ vectorisation of the function `mapN2p.m` that i) interpolates updated nodal solutions to the material points (velocities and coordinates) and ii) the double mapping (DM or MUSL) procedure (see ~~Fern et al. (2019)~~ Fern et al. 2019). The material point velocity \underline{v}_p is defined as an interpolation of the solution of the updated nodal accelerations, given by:

$$\underline{v}_p^{t+\Delta t} = \underline{v}_p^t + \Delta t \sum_{\underline{I}=1}^{n_{Ne}} \sum_{\underline{n}=1}^{n_n} S_{\underline{I}\underline{n}}(\underline{x}_p) \underline{a}_{\underline{I}\underline{n}}^{t+\Delta t}. \quad (21)$$

The material point updated momentum is found by $\underline{p}_p^{t+\Delta t} = m_p \underline{v}_p^{t+\Delta t}$. The double mapping procedure (~~MUSL~~) of the nodal velocity \underline{v}_n consists of the remapping of the updated material point momentum on the mesh, divided by the nodal mass, which yields the nodal incremental displacements $\Delta \underline{u}_I$ when multiplied by an increment of time, both given by:

$$\underline{v}_{\underline{I}\underline{n}}^{t+\Delta t} = m_{\underline{I}\underline{n}}^{-1} \sum_{p \in \underline{I} \underline{p} \in \underline{n}} S_{\underline{I}\underline{n}}(\underline{x}_p) \underline{p}_p^{t+\Delta t}, \underline{\Delta t}_{\underline{I}} = \underline{\Delta t}_{\underline{I}}^{t+\Delta t} \quad (22)$$

and for which boundary conditions are enforced.

Finally, the material point coordinates are updated based on the following:

$$\mathbf{x}_p^{t+\Delta t} = \mathbf{x}_p^t + \Delta t \sum_{I=1}^{n_{Ne}} \sum_{n=1}^{n_n} S_{In}(\mathbf{x}_p) \Delta_I \mathbf{v}_n^{t+\Delta t}. \quad (23)$$

To solve for the interpolation of the updated nodal solutions to the material points, we rely on a combination of **elementwise** **element-wise** matrix multiplication between the array of basis functions `mpD.S` with the global vectors through a transform of the `p2N` array, i.e., `iDx=meD.DoF*p2N-1` and `iDy=iDx+1` (Lines 3-4 in Code Fragment 3 in Fig. 7), which are used to access to x and y components of global vectors.

When accessing global nodal vectors by means of `iDx` and `iDy`, the resulting arrays are naturally of the same size as `p2N` and are therefore dimension-compatible with `mpD.S`. For instance, a summation along the columns (e.g., the associated nodes of material points) of an **elementwise** **element-wise** multiplication of `mpD.S` with `meD.a(iDx)` results in an interpolation of the x-component of the global acceleration vector to the material points.

This procedure is used for the velocity update (Lines 6-7 Line 6 in Fig. 7) and for the material point coordinate update (Line 11-10 in Fig. 7). A remapping of the nodal momentum is carried out (Lines 17 to 20 12 to 16 in Fig. 7), which allows calculating the updated nodal incremental displacements (Line 22-17 in Fig. 7). Finally, boundary conditions of nodal incremental displacements are enforced (Lines 29-32 21-22 in Fig. 7).

```

1 function [meD,mpD] = mapN2p(meD,mpD,dt,l2g,p2N,bc)
2 %% INTERPOLATE SOLUTIONS N to p
3 iDx = meD.DoF*p2N-1 ;%
4 iDy = iDx+1 ;%
5 % VELOCITY UPDATE
6 mpD.v = mpD.v+dt*[sum(mpD.S.*meD.a(iDx),2) sum(mpD.S.*meD.a(iDy),2)] ;%
7 % MOMENTUM UPDATE
8 mpD.p = mpD.v.*repmat(mpD.m,1,meD.DoF) ;%
9 %% UPDATE NODAL MOMENTUM WITH UPDATED MP MOMENTUM (MUSL OR DOUBLE MAPPING)
10 meD.p(:) = 0.0 ;%
11 p = reshape([mpD.S.*repmat(mpD.p(:,1),1,meD.nNe) ;...
12             mpD.S.*repmat(mpD.p(:,2),1,meD.nNe)] ,...
13             mpD.n*meD.nDoF(1),1) ;%
14 meD.p = accumarray(l2g(:),p,[meD.nDoF(2) 1]) ;%
15 meD.u = dt*(meD.p./meD.mr) ;%
16 iD = meD.mr==0 ;%
17 meD.u(iD) = 0.0 ;%
18 %% BOUNDARY CONDITIONS: FIX DIRICHLET BOUNDARY CONDITIONS
19 meD.u(bc.x(:,1))=bc.x(:,2) ;%
20 meD.u(bc.y(:,1))=bc.y(:,2) ;%
21 %% UPDATE COORDINATE AND DISPLACEMENT
22 mpD.x = mpD.x+[sum(mpD.S.*meD.u(iDx),2) sum(mpD.S.*meD.u(iDy),2)] ;%
23 mpD.u = mpD.u+[sum(mpD.S.*meD.u(iDx),2) sum(mpD.S.*meD.u(iDy),2)] ;%
24 end

```

Figure 7. Code Fragment 3 shows the **vectorized** **vectorised** solution for the interpolation of nodal solutions to material points with a double mapping procedure (or MUSL) within the function `mapN2p.m`.

3.4 Initial settings and adaptive time step

Regarding the initial setting of the background mesh of the demonstration cases further presented, we select a uniform mesh and a regular distribution of material points within the initially populated elements of the mesh. Each element is evenly filled with 4 material points, e.g., $n_{pe} = 2^2$, unless otherwise stated.

370 In this contribution, Dirichlet boundary conditions are resolved directly on the background mesh, as in the standard finite element method. This implies that boundary conditions are resolved only in contiguous regions between the mesh and the material points. Deviating from this contiguity or having the mesh not aligned with the coordinate system requires specific treatments for boundary conditions (Cortis et al., 2018). Furthermore, we ignore the external tractions as their implementation is complex.

375 As explicit time integration is only conditionally stable, any explicit formulation requires a small time step Δt to ensure numerical stability (Ni and Zhang, 2020), e.g., smaller than a critical value defined by the Courant-Friedrich-Lewy (CFL) condition. Hence, we employ an adaptive time step (de Vaucorbeil et al., 2020), which considers the velocity of the material points. The first step is to compute the maximum wave speed of the material using (Zhang et al., 2016; Anderson Jr, 1987)

$$(c_x, c_y) = \left(\max_p (V + |(v_x)_p|), \max_p (V + |(v_y)_p|) \right), \quad (24)$$

380 where the wave speed is $V = ((K + 4G/3)/\rho)^{\frac{1}{2}}$, K and G are the bulk and shear moduli respectively, ρ is the material density, $(v_x)_p$ and $(v_y)_p$ are the material point velocity components. Δt is then restricted by the CFL condition as followed:

$$\Delta t = \alpha \min \left(\frac{h_x}{c_x}, \frac{h_y}{c_y} \right), \quad (25)$$

where $\alpha \in [0; 1]$ is the time step multiplier, and h_x and h_y are the mesh spacings.

4 Results

385 In this section, we first demonstrate our MATLAB-based MPM solver to be efficient in reproducing results from other studies, i.e., the compaction of an elastic column (Coombs et al., 2020) (e.g., quasi-static analysis), the cantilever beam problem (Sadeghirad et al., 2011) (e.g., large elastic deformation) and an application to landslide dynamics (Huang et al., 2015) (e.g., elasto-plastic behaviour). Then, we present both the efficiency and the numerical performances for a selected case, e.g., the elasto-plastic collapse. We conclude and compare the performances of the solver with respect to the specific case of an impact
390 of two elastic disks previously implemented in a Julia language environment by (Sinaie et al., 2017).

Regarding the performance analysis, we investigate the performance gain of the vectorised solver considering a double arithmetic precision with respect to the total number of material point because of the following reasons: i) the mesh resolution, i.e., the total number of elements n_{el} , influences the wall-clock time of the solver by reducing the time step due to the CFL condition hence increasing the total number of iterations. In addition, ii) the total number of material points n_p increases
395 the number of operations per cycle due to an increase of the size of matrices, i.e., the size of the strain-displacement matrix depends on n_p and not on n_{el} . Hence, n_p consistently influences the performance of the solver whereas n_{el} determines the wall-clock time of the solver. The performance of the solver is addressed through both the number of floating point operations per second (flops), and by the average number of iteration per second (it/s). The number of floating point operations per second was manually estimated for each function of the solver.

4.1.1 Convergence: elastic compaction under self-weight of a column

Following the convergence analysis proposed by Wang et al. (2019); Charlton et al. (2017) Coombs and Augarde (2020); Wang et al. (2019), we analyse an elastic column of an initial height $l_0 = 10$ m subjected to an external load (e.g. the gravity). We selected the cpGIMPM variant with a domain update based on the diagonal components of the deformation gradient. Coombs et al. (2020) showed that such domain update is well suited for hydrostatic compression problems. We also selected the CPDI2q variant as a reference, because of its superior convergence accuracy for such problem compared to GIMPM (Coombs et al., 2020).

The initial geometry is shown in Fig. 8. The background mesh is made of a bi-linear four-noded quadrilateral quadrilaterals, and roller boundary conditions are applied on the base and the sides of the column, initially populated by 4 material points per element. The column is 1 element wide and n elements tall and, the number of element in the vertical direction is increased from 1 to a maximum of 1280 elements. The time step is adaptive and we selected a time step multiplier of $\alpha = 0.5$, e.g., minimal and maximal time step values of $\Delta t_{\min} = 3.1 \cdot 10^{-4}$ s and $\Delta t_{\max} = 3.8 \cdot 10^{-4}$ s respectively for the finest mesh of 1280 elements.

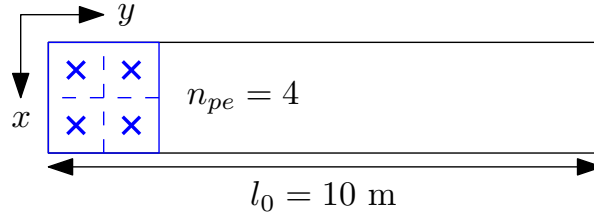


Figure 8. Initial geometry of the column.

To consistently apply the external load for the explicit solver, we follow the recommendation of Bardenhagen and Kober (2004), i.e., a quasi-static solution (given an explicit integration scheme is chosen) is obtained if the total simulation time is equal to 40 elastic wave transit times. The material has an elastic modulus $E = 1 \cdot 10^6$ Pa and a Young's modulus $E = 1 \cdot 10^4$ Pa and a Poisson's ratio $\nu = 0$ with a density $\rho = 80 \text{ kg m}^{-3}$. The gravity g is increased from 0 to its final value, i.e., $g = 9.81 \text{ m s}^{-2}$. We performed additional implicit quasi-static simulations (named iCPDI2q) in order to consistently discuss the results with respect to what was reported in Coombs and Augarde (2020). The external force is consistently applied over 25-50 equal load steps. The vertical normal stress is given by the analytical solution (Coombs and Augarde, 2020) $\sigma_{yy}(y_0) = \rho g(l_0 - y_0)$, where l_0 is the initial height of the column and y_0 is the initial position of a point within the column.

The error between the analytical and numerical solutions is as follows:

$$\text{error} = \sum_{p=1}^{n_p} \frac{|(\sigma_{yy})_p - \sigma_{yy}(y_p)| (V_0)_p}{(\rho g l_0) V_0}, \quad (26)$$

where $(\sigma_{yy})_p$ is the vertical stress stress along the y -axis of a material point p (Fig. 8) of an initial volume $(V_0)_p$ and V_0 is the initial volume of the column, i.e., $V_0 = \sum_{p=1}^{n_p} (V_0)_p$.

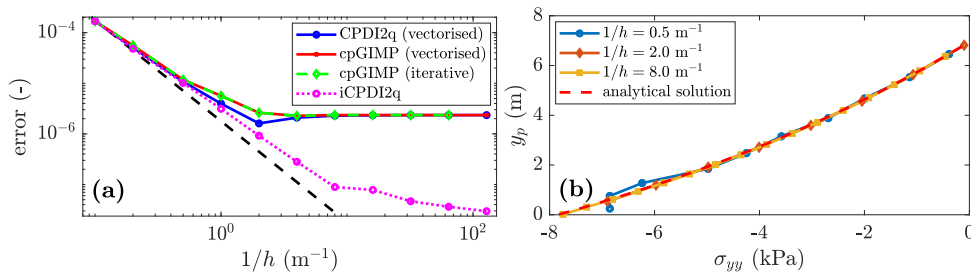


Figure 9. Linear convergence a) Convergence of the error: a limit is reached at error $\approx 2 \cdot 10^{-6}$ for the explicit solver, whereas the quasi-static solution still converges. This was already demonstrated in Bardenhagen and Kober (2004) as an error saturation due to the explicit scheme, i.e., the equilibrium is never resolved. b) The stress σ_{yy} along the y -axis predicted at the deformed position y_p by the CPDI2q variant is in good agreements with the analytical solution for a refined mesh.

425 The convergence toward a quasi-static solution is shown in Fig. 9. ~~As mentioned by Coombs et al. (2020), it is linear for both~~
~~epGIMP (a). It is quadratic for both cpGIMP and CPDI2q, but contrary to ?Coombs et al. (2020) Coombs et al. (2020); Coombs and Aug~~
 who reported a full convergence, it stops at error $\approx 2 \cdot 10^{-6}$ for the explicit implementation. This was already outlined by Bar-
 denhagen and Kober (2004) as a saturation of the error caused by resolving the dynamic stress wave propagation, which is
 inherent to any explicit scheme. Hence, a static solution could never be achieved because, unlike quasi-static implicit methods,
 430 the elastic waves propagate indefinitely and the static equilibrium is never resolved. This is consistent when compared to the
~~iCPDI~~ ~~iCPDI2q~~ solution we implemented (green circles), whose behaviour is still converging below the limit error $\approx 2 \cdot 10^{-6}$
 reached by the explicit solver. ~~In addition However, the convergence becomes quadratic below this limit. It confirms that the~~
~~error saturation is due to the explicit format and not to our numerical implementation. rate of the implicit algorithm decreases~~
~~as the mesh resolution increases. We did not investigate this since our focus is on the explicit implementation. The vertical~~
 435 ~~stresses of material points are in good agreements with the analytical solution (see Fig. 9 b)). Some oscillations are observed~~
~~for a coarse mesh resolution but these rapidly decrease as the mesh resolution increases.~~

4.2 Large deformation: the elastic cantilever beam problem

We finally report the wall-clock time for the cpGIMP (iterative), cpGIMP (vectorised) and the CPDI2q (vectorised)
 variants. As claimed by Sadeghirad et al. (2013, 2011), the CPDI2q variant induces no significant computational cost compared
 440 to the cpGIMP variant. However, the absolute value between vectorised and iterative implementations is significant. For
 $n_p = 2560$, the vectorised solution completed in 1161 s whereas the iterative solution completed in 52'856 s. The vectorised
 implementation is roughly 50 times faster than the iterative implementation.

4.1.1 Large deformation: the elastic cantilever beam problem

The cantilever beam problem ~~Sinaie et al. (2017); Sadeghirad et al. (2011)~~ (Sinaie et al., 2017; Sadeghirad et al., 2011) is the
 445 second benchmark which demonstrates the robustness of the MPM solver. Two MPM variants are implemented, namely,

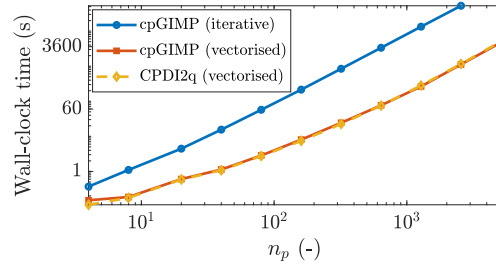


Figure 10. Wall-clock time for cpGIMP (vectorised and iterative solutions) and the CPDI2q solution with respect to the total number of material points n_p . There is no significant differences between CPDI2q and cpGIMP variants regarding the wall-clock time. The iterative implementation is also much slower than the vectorised implementation.

i) the contiguous ~~GIMP~~ (epGIMP cpGIMP) which relies on the stretch part of the deformation gradient (see ~~Charlton et al. (2017)~~ Charlton et al. 2017) to update the particle domain ~~since large rotations are expected during the deformation of the beam~~, and ii) the convected particle domain interpolation (CPDI ~~Leavy et al. (2019); Sadeghirad et al. (2011)~~). In addition, ~~two~~, Leavy et al. 2019; Sadeghirad et al. 2011). We selected the CPDI variant since it is more suitable to large torsional deformation modes (Coombs et al., 2020) than the CPDI2q variant. Two constitutive elastic models are selected, i.e., neo-Hookean Guilkey and Weiss (2003) or linear elastic York et al. (1999) solids. For consistency, we use the same physical quantities as in Sadeghirad et al. (2011), i.e., an elastic modulus $E = 10^6$ Pa, a Poisson's ratio $\nu = 0.3$, a density $\rho = 1050$ kg/m³, the gravity $g = 10.0$ m/s and a real-time simulation $t = 3$ s with no damping forces introduced.

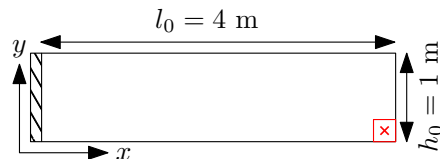


Figure 11. Initial geometry for the cantilever beam problem; the free end material point appears in red where a red cross marks its centre.

The beam geometry is depicted in Fig. 11 and is discretized by 64 ~~bi-linear~~ four-noded quadrilaterals, each of them initially populated by ~~3² 9~~ material points (e.g., $n_p = 576$) with a ~~adaptive~~ time step determined by the CFL condition, ~~e.g., $\Delta t = 10^{-3}$ s~~ i.e., the time step multiplier is $\alpha = 0.1$, which yields minimal and maximal time step values of $\Delta t_{\min} = 5.7 \cdot 10^{-4}$ s and $\Delta t_{\max} = 6.9 \cdot 10^{-4}$ s respectively. The large deformation is initiated by suddenly applying the gravity at the beginning of the simulation, i.e., $t = 0$ s.

As indicated in Sadeghirad et al. (2011), the ~~epGIMP~~ cpGIMP simulation failed when using the diagonal components of the deformation gradient to update the material point domain. ~~However, i.e., the domain vanishes under large rotations as stated in (Coombs et al., 2020). However and as~~ as expected, the ~~epGIMP~~ cpGIMP simulation succeeded when using the diagonal terms of the stretch part of the deformation ~~tensor~~ gradient, as proposed by ~~Charlton et al. (2017)~~ Coombs et al. (2020); Charlton et al. (2017). The numerical solutions, obtained by the latter ~~epGIMP~~ cpGIMP and CPDI, to the vertical deflection Δu of the material

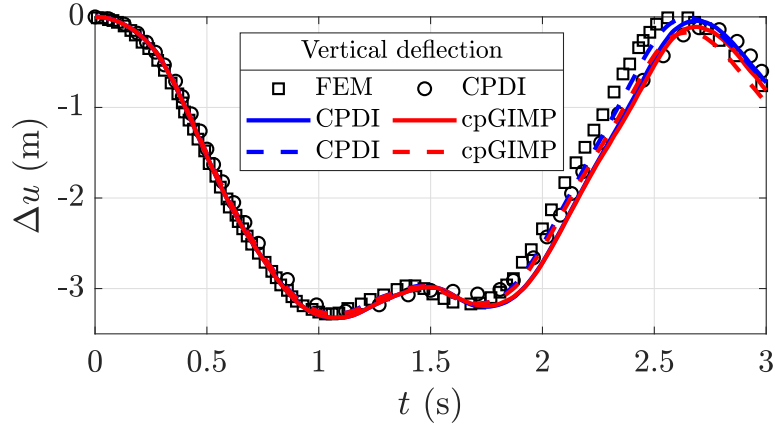


Figure 12. Vertical deflection Δu for the cantilever beam problem. The black markers denote the solutions of Sadeghirad et al. (2011) (circles for CPDI and squares for FEM). The line colour indicates the MPM variant (blue for CPDI and red for cpGIMP), solid lines refer to a linear elastic solid, whereas dashed lines refer to a neo-Hookean solid. The vertical deflection Δu corresponds to the vertical displacement of the bottom material point at the free end of the beam (the red cross in Fig. 11).

point at the bottom free end of the beam (e.g., the red cross in Fig. 11) are shown in Fig. 12. Some comparative results reported
 465 by Sadeghirad et al. (2011) are depicted by black markers (squares for the FEM solution and circles for the CPDI solution),
 whereas the results of our MPM solver are depicted by lines.

The local minimal and the minimal and maximal values (in timing and magnitude) are in agreement with the FEM solution
 of Sadeghirad et al. (2011). Moreover, the elastic response is in agreement with the CPDI results reported by Sadeghirad
 et al. (2011) but, it differs in timing with respect to the FEM solution. This confirms our numerical implementation of CPDI
 470 when compared to the one proposed by Sadeghirad et al. (2011). In addition, the elastic response does not substantially differ
 from a linear elastic solid to a neo-Hookean one. It demonstrates the incremental implementation of the MPM solver to be
 relevant in capturing large elastic deformations for the cantilever beam problem.

4.2 Elasto-plasticity: the column-collapse

We compare our MPM solver with a non-associated plasticity based on a Drucker-Prager model with tension cutoff (Huang et al. (2015)
 475) to the experimental results of an elasto-plastic collapse of a material (e.g., an aluminium bar assemblage, see Bui et al. (2008)
). The numerical implementation is detailed in Huang et al. (2015), and we therefore suggest the interested reader to directly
 refer to their contribution since we do not describe the elasto-plastic model in this manuscript. Figure 13 shows the finite
 deformation of the material point domain, i.e., a) or c), and, the vertical Cauchy stress field, i.e., b) or d), for CPDI and
 cpGIMP. The stress oscillations due to the cell-crossing error are partially cured when using a domain-based variant compared
 480 to the standard MPM. However, spurious vertical stresses are more developed in Fig. 13 (d) compared to Fig. 13 (b) where the

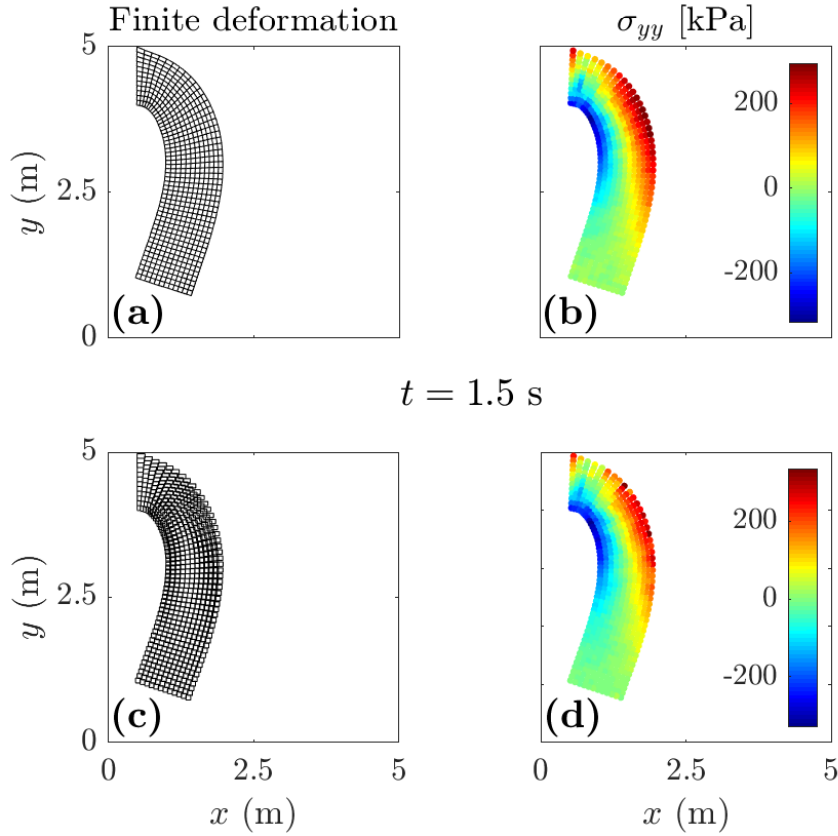


Figure 13. Finite deformation of the material point domain and vertical Cauchy stress σ_{yy} for CPDI, i.e., a) & b), and for cpGIMP, i.e., c) & d). The CPDI variant gives a better and contiguous description of the material point's domain and a slightly smoother stress field, compared to the cpGIMP variant, which is based on the stretch part of the deformation gradient.

vertical stress field appears even smoother. Both CPDI and cpGIMP give a decent representation of the actual geometry of the deformed beam.

Our elasto-plastic MPM solver closely follows the implementation of Huang et al. (2015), except our solver relies on an MUSL procedure, whereas Huang et al. (2015) selected the USF procedure. The We also report a quite significant difference in execution time between the CPDI variant compared to the CPDI2q and cpGIMP variants, i.e., CPDI executes in an average 280.54 it/s whereas both CPDI2q and CPGIMP execute in an average 301.42 it/s and an average 299.33 it/s, respectively.

4.1.1 Application: the elasto-plastic slumping dynamics

We present an application of the MPM solver (vectorised and iterative version) to the case of landslide mechanics. We selected the domain-based CDPI variant since it performs better than the CPDI2q variant in modelling torsional and stretch deformation modes (Wang et al., 2019) coupled to an elasto-plastic problem is solved by i) an elastic trial, ii) corrected by a return-mapping

when the material yields either in shear or in tension or both, assuming a constitutive model based on a non-associated (the dilation angle $\psi = 0$) perfectly plastic behaviour of the material. Since the MPM variant in Huang et al. (2015) was not clearly stated, we use the uGIMP variant. The reason is the collapse results in extreme deformations, for which a domain update based on the deformation gradient systematically resulted in a failure during the simulation. We conducted preliminary investigations and concluded that the uGIMP variant was the most reliable MPM variant for such a problem. Mohr-Coulomb (M-C) plasticity (Simpson, 2017). We i) analyse the geometrical features of the slump and, ii) compare the results (the geometry and the failure surface) to the numerical simulation of Huang et al. (2015), which is based on a Drucker-Prager model with tension cut-off (D-P).

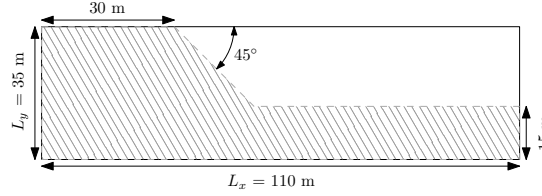


Figure 14. Initial geometry for the elasto-plastic-collapse (slump problem from Huang et al. (2015)). Roller boundaries boundary conditions are imposed on the left and right boundaries of the domain while a no-slip condition is enforced at the bottom of the domain. The aluminium-bar assemblage has dimensions base of $l_0 \times h_0$ and is discretized by $n_{pe} = 4$ material points per element, and Table ?? summarizes the material properties.

The initial geometry and boundary conditions used for this problem are depicted

500 The geometry of the problem is shown in Fig. 16, while the parameters used are summarized in Table ?? and represent the problem described in Bui et al. (2008). The aluminium assemblage 14, the soil material is discretized by $n_p = 28'800$ material points within a mesh made of 320×48 quadrilateral elements 110×35 elements with $n_{pe} = 9$, resulting in a uniform spacing of $h = 1.25$ mm. The time step is given by the CFL condition, e.g., $\Delta t = 7.02 \cdot 10^{-5}$ s for a total simulation time of 1.25 s.

Parameters used for the elasto-plastic collapse simulation. The values of parameters are those found in Huang et al. (2015),
 505 obtained using a shear box test by Bui et al. (2008). Parameter Symbol Value Unit Density ρ 2650 kgm^{-3} $n_p = 21'840$ material points. A uniform mesh spacing $h_{x,y} = 1$ m is used and, rollers are imposed at the left and right domain limits while a no-slip condition is enforced at the base of the material. We closely follow the numerical procedure proposed in Huang et al. (2015), i.e., no local damping is introduced in the equation of motion and the gravity is suddenly applied at the beginning of the simulation. As in Huang et al. (2015), we consider an elasto-plastic cohesive material of density $\rho = 2100 \text{ kg}\cdot\text{m}^{-3}$, with an
 510 elastic modulus $E = 70 \text{ MPa}$ and a Poisson's ratio $\nu = 0.3$ Bulk modulus $K = 0.7 \text{ MPa}$ Cohesion $c = 0 \text{ Pa}$ Internal friction angle $\phi = 19.8^\circ$ Dilation angle $\psi = 0^\circ$ Gravity $g = 9.81 \text{ m}\cdot\text{s}^{-2}$

Figure 17 shows the numerical solution compared with the experimental results of Bui et al. (2008). We observe a good agreement between the numerical simulation and the experiments, considering either the final surface (blue square dotted line) or the failure surface (blue circle dotted line). Similarly, the repose angle in the numerical simulation is approximately 13° from the horizontal, which is also in agreement with the experimental data reported by Bui et al. (2008) (e. g. $\nu = 0.3$. The cohesion

is $c = 10$ Pa, the internal friction angle is $\phi = 20^\circ$ with no dilatancy, i.e., the dilatancy angle is $\psi = 0$. The total simulation time is 7.22 s and, they reported a final angle of 14°), we select a time step multiplier $\alpha = 0.5$. The adaptive time steps (considering the elastic properties and the mesh spacings $h_{x,y} = 1$ m) yield minimal and maximal values $\Delta t_{\min} = 2.3 \cdot 10^{-3}$ s and $\Delta t_{\max} = 2.4 \cdot 10^{-3}$ s respectively.

520 These numerical results demonstrate the solver to be in agreement with both previous experimental (Bui et al. (2008)) and numerical results (Huang et al. (2015)) and confirms its ability to solve

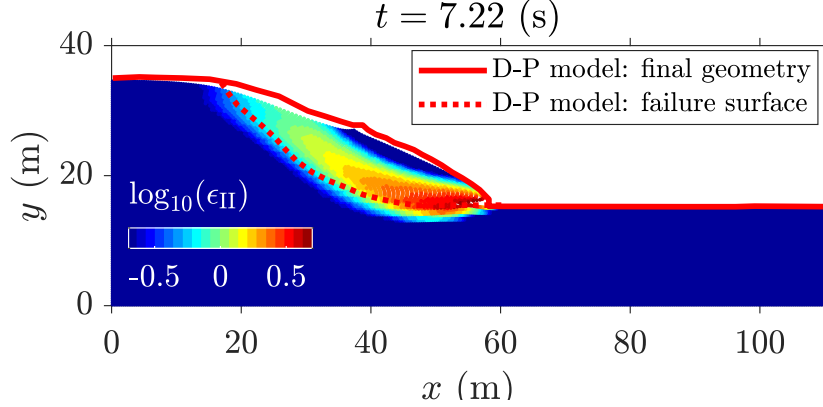


Figure 15. MPM solution to the elasto-plastic slump. The red lines indicate the numerical solution of Huang et al. (2015) and, the coloured points indicate the second invariant of the accumulated plastic strain ϵ_{II} obtained by the CPDI solver. An intense shear zone progressively develops backwards from the toe of the slope, resulting in a circular failure mode.

The numerical solution to the elasto-plastic problems such as granular collapses using an appropriate constitutive model. However, it also demonstrates the inability of the MPM variants based on a domain update (GIMPM or CPDI) to resolve extremely large plastic deformations when relying on the normal components of problem is shown in Fig. 15. An intense shear zone, highlighted by the second invariant of the deformation gradient or its stretch part to update the material point domain (interested readers are referred to the contribution of Coombs et al. (2020) regarding the suitability of different domain update variants). Consecutively, we performed an additional simulation using a domain update based on the determinant of the deformation gradient. No significant differences were observed with the experimental results, and the simulation succeeded accumulated plastic strain ϵ_{II} , develops at the toe of the slope as soon as the material yields and propagates backwards to the top of the material. It results in a rotational slump. The failure surface is in good agreement with the solution reported by Huang et al. (2015) (continuous and discontinuous red lines in Fig. 15) but, we also observe differences, i.e., the crest of the slope is lower compared to the original work of Huang et al. (2015). This may be explained by the problem of spurious material separation when using sMPM or GIMPM (Sadeghirad et al., 2011), the latter being overcome with the CPDI variant, i.e., the crest of the slope experiences considerable stretch deformation modes. Despite some differences, our numerical results appear coherent with those reported by Huang et al. (2015).

The vectorised and iterative solutions are resolved within approximately 630 s (a wall-clock time of ≈ 10 min. and an average 4.20 it/s) and 14'868 s (a wall-clock time of ≈ 4.1 hrs. and an average 0.21 it/s) respectively. This corresponds to a performance gain of 23.6. The performance gain is significant between an iterative and a vectorised solver for this problem.

Final geometry of the collapse: in the intact (undeformed) region, the material points are coloured in green, whereas in deformed regions, they are coloured in red and indicate plastic deformations of the initial mass. The transition between the deformed and undeformed region marks the failure surface of the material. Experimental results are depicted by the blue dotted lines.

4.2 Computational efficiency: loop-based code versus vectorized code performance

4.2.1 Iterative and vectorised elasto-plastic collapses

We evaluate the computational efficiency of the MATLAB-based MPM performance of the solver, using the MATLAB version R2018a on an Intel Core i7-4790, with a benchmark based on the collapse of an elasto-plastic collapse of the aluminium-bar assemblage, for which numerical and experimental results were initially reported by Bui et al. (2008) and Huang et al. (2015) respectively.

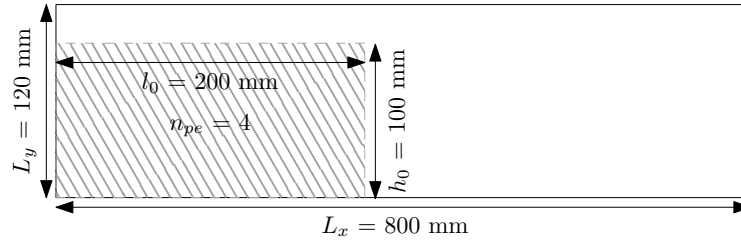


Figure 16. Initial geometry for the elasto-plastic collapse (Huang et al., 2015). Roller boundaries are imposed on the left and right boundaries of the computational domain while a no-slip condition is enforced at the bottom of the domain. The aluminium-bar assemblage has dimensions of $l_0 \times h_0$ and is discretized by $n_{pe} = 4$ material points per initially populated element.

We vary the number of elements of the background mesh, which results in a variety of different mesh spacings h regular mesh spacings $h_{x,u}$. The number of elements along the x-direction is $n_{el,x} = [20, 40, 80, 160, 320, 640]$, and the resulting number of elements in the y-direction is $n_{el,y} = [2, 5, 11, 23, 47, 95]$. x- and y- directions are $n_{el,x} = [10, 20, 40, 80, 160, 320, 640]$ and $n_{el,y} = [1, 2, 5, 11, 23, 47, 95]$ respectively. The number of material points per element is kept constant, i.e., $n_{pe} = 3^2$, and the $n_{pe} = 4$, and this yields a total number of material points is $n_p = [128, 465, 1830, 7260, 28'920, 115'440]$. $n_p = [10, 50, 200, 800, 3'200, 12'800]$. The initial geometry and boundary conditions used for this problem are depicted in Fig. 16. The total simulation time is 1.0 s and, the time step multiplier is $\alpha = 0.5$. Accordingly to Huang et al. (2015), the gravity $g = 9.81 \text{ m}\cdot\text{s}^{-2}$ is applied to the assemblage and, no damping is introduced. We consider a non-cohesive granular material (Huang et al., 2015) of density $\rho = 2650 \text{ kg}\cdot\text{m}^3$, with a bulk modulus $K = 0.7 \text{ MPa}$ and a Poisson's ratio $\nu = 0.3$. The cohesion is $c = 0 \text{ Pa}$, the internal friction angle is $\phi = 19.8^\circ$ and there is no dilatancy, i.e., $\psi = 0$.

We calculate the average number of iterations per second (conducted preliminary investigations using either uGIMP or cpGIMP variants, the latter with a domain update based either on the determinant of the deformation gradient or on the diagonal components of the stretch part of the deformation gradient. We concluded the uGIMP was the most reliable, even though its suitability is restricted to both simple shear and pure rotation deformation modes (Coombs et al., 2020).

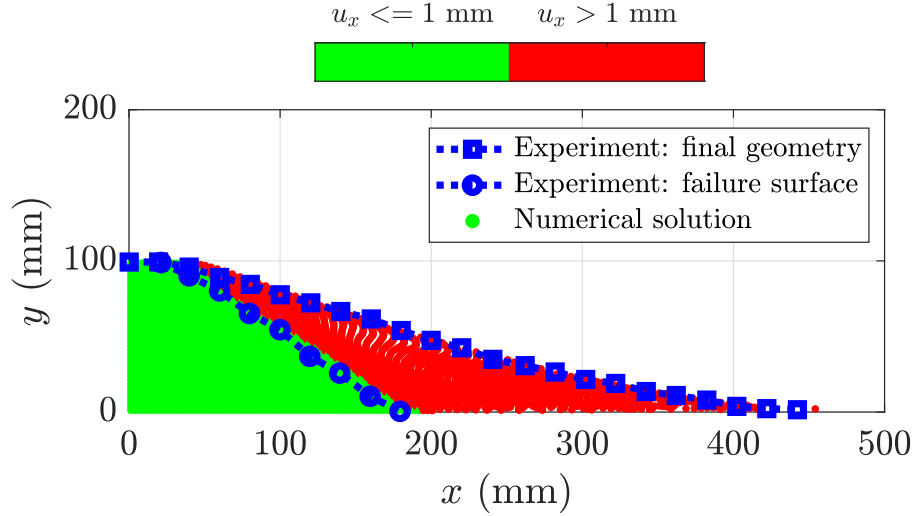


Figure 17. Final geometry of the collapse: in the intact region (horizontal displacement $u_x < 1$ mm), the material points are coloured in green, whereas in the deformed region (horizontal displacement $u_x > 1$ mm), they are coloured in red and indicate plastic deformations of the initial mass. The transition between the deformed and undeformed region marks the failure surface of the material. Experimental results of (Bui et al., 2008) are depicted by the blue dotted lines. The computational domain is discretized by a background mesh made of 320×48 quadrilateral elements with $n_p = 4$ per initially populated element, i.e., a total $n_p = 12'800$ material points discretize the aluminium assemblage.

We observe a good agreement between the numerical simulation and the experiments (see Fig. 17), considering either the final surface (blue square dotted line) or the failure surface (blue circle dotted line). The repose angle in the numerical simulation is approximately 13° , which is in agreements with the experimental data reported by Bui et al. (2008), e.g., they reported a final angle of 14° .

The vectorised and iterative solutions (for a total of $n_p = 12'800$ material points) are resolved within approximately 1595 s (a wall-clock time of ≈ 0.5 hrs. and an average 10.98 it/s) and 43'861 s (a wall-clock time of ≈ 12 hrs. and an average 0.38 it/s) which corresponds to the number of calculation cycles during 1 second for an increasing total number of elements. We use this metric since it provides a clearer insight regarding the efficiency of the numerical solver, i.e., the more iterations there are, the more efficient the solver. Figure ?? shows an overall speed-up ratio of 20 reached by the vectorized solver(s) respectively. This corresponds to a performance gain of 28.24 for a vectorised code over an iterative code to solve this elasto-plastic problem.

The performance of the solver is demonstrated in Fig. 18. A peak performance of ≈ 900 Mflops is reached, as soon as n_p exceeds 1000 material points and, a residual performance of ≈ 600 Mflops is further resolved (for $n_p \approx 50'000$ material points). Every functions provide an even and fair contribution on the overall performance, except the function `constitutive.m` for which the performance appears delayed or shifted. First of all, this function treats the elasto-plastic constitutive relation, in which the dimensions of the matrices are smaller when compared to the `iterative-implementation`. Such a gain is appreciable since it results in a decrease of the runtime, i.e., approximately 40 hours for the iterative version, whereas the vectorized solution is achieved in 3 hours ($n_p = 115'440$) other functions. Hence, the amount of floating point operations per second is lower compared to other functions, e.g., `p2Nsolve.m`. This results in less performance for an equivalent number of material points. It also requires a greater number of material points to increase the dimensions of the matrices in order to exceed the L2 cache maximum capacity.

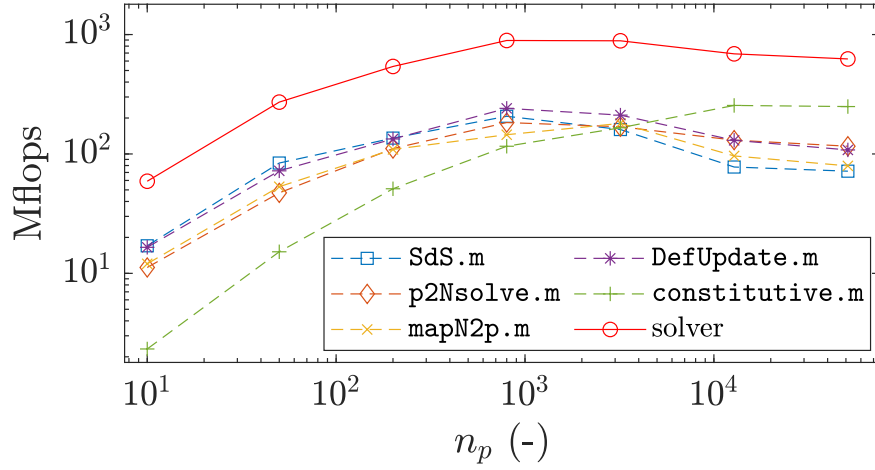


Figure 18. Number of iterations floating point operation per second, i.e., seconds (flops) with respect to the total number of calculation cycles achieved in one second with respect material point n_p for the vectorised implementation. The discontinuous lines refer to the mesh-spacing h under functions of the MATLAB version R2018a solver, whereas the continuous line refer to the solver. A peak performance of 900 Mflops is reached by the solver for $n_p > 1000$ and, a residual performance of 600 Mflops is further resolved for an increasing n_p .

In addition, we also monitor the average time spent on the different functions called during a single execution cycle \bar{t}_c (Fig. ??). When comparing time spent on the functions `p2Nsolve.m` and `mapN2p.m`, we report a speed-up of 24 and 22, respectively. This difference is expected since these functions originally necessitate an extensive use of two nested for-loops to calculate i) the material point contribution or ii) the interpolation of updated nodal solutions. This considerations provide a better understanding of the performance gain of the vectorised solver showed in Fig. 19: the gain increases and then, reaches a plateau and ultimately, decreases to a residual gain. This is directly related to the peak and the residual performances of the solver showed in Fig. 18.

We conclude with a direct comparison of a vectorized

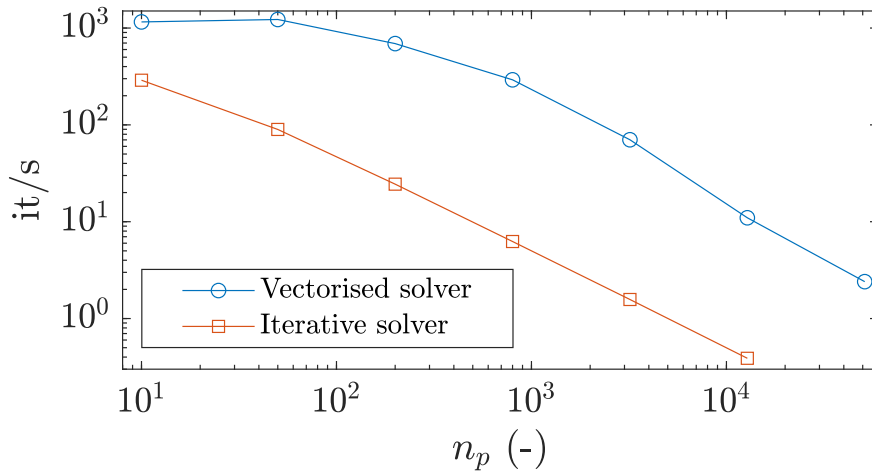


Figure 19. Average time \bar{t}_c spent on Number of iterations per second with respect to the functions called during one calculation cycle for total number of material point n_p . The greatest performance gain is reached around $n_p = 1000$, which is related to the iterative and peak performance of the vectorized solver for $n_p = 115'440$ (see Fig. 18). The gains corresponding to the peak and residual performances are 46 and 28 respectively.

4.2.2 Comparison between Julia and MATLAB

We compare the computational efficiency of the vectorised CPDI2q implementation of the collision of two elastic disks MATLAB implementation and the computational efficiency reported by Sinaie et al. (2017) of a Julia-based implementation of the collision of two elastic disks problem. However, we note a difference between the actual implementation and the one used by Sinaie et al. (2017); the latter is based on a USL variant with a cutoff cut-off algorithm, whereas our the present implementation relies on the MUSL (or double mapping) procedure, which necessitates a double mapping procedure. The initial geometry and parameters are the same as those used in Sinaie et al. (2017). However, the time step is adaptive and, we select a time step multiplier $\alpha = 0.5$. Given the variety of mesh resolution, we do not present minimal and maximal time step values.

Our CPDI2q implementation, in MATLAB R2018a, is, ad-minimaat least, 2.8 times faster than the Julia implementation proposed by Sinaie et al. (2017) for similar hardware (see Table 1). Sinaie et al. (2017) completed the analysis with an Intel Core i7-6700 (4 cores with a base frequency of 3.40 GHz up to a turbo frequency of 4.00 GHz) with 16 GB RAM, whereas we used an Intel Core i7-4790 with similar specifications (see section-Section 2). However, the performance ratio between MATLAB and Julia seems to decrease as the mesh resolution increases.

4.3 Elasto-plastic slumping

We present an application of the MPM solver to the case of landslide mechanics. Considering a CPDI2q variant coupled to an elasto-plastic constitutive model based on a Mohr-Coulomb (M-C) non-associated plasticity Simpson (2017), we analyse the

Table 1. Efficiency comparison of the Julia implementation of Sinaie et al. (2017), and the MATLAB-based implementation for the two elastic disk impact problems.

mesh	n_{pe}	n_p	Its/s		Gain
			Julia	MATLAB	
20×20	2^2	416	132.80	224.45 <u>450.27</u>	<u>3.40</u>
20×20	4^2	1'624	33.37	81.07 <u>118.45</u>	<u>3.54</u>
40×40	2^2	1'624	26.45	77.61 <u>115.59</u>	<u>4.37</u>
80×80	4^2	25'784	1.82	4.57 <u>5.21</u>	<u>2.86</u>

geometrical features of the slump and ii) compare the results (the geometry and the failure surface) to the numerical simulation of Huang et al. (2015), which is based on a Drucker-Prager model with tension cutoff (D-P).-

Initial geometry for the slump problem from Huang et al. (2015). Roller boundary conditions are imposed on the left and right of the domain while a no-slip condition is enforced at the base of the material.

Since an explicit scheme is used, we introduce a local damping in the equations of motion to resolve the equilibrium during a loading phase of 8 seconds, during which the gravity g is linearly ramped up to 9.81 m s^{-2} . The elasto-plastic behaviour is activated once this loading procedure is terminated, and the simulation proceeds during 7 additional seconds for a total simulation time of 15 seconds. The local damping coefficient is set to 0.1 since the latter damps the oscillations while preserving the dynamics Wang et al. (2016c).-

Parameters used for the elasto-plastic slump. The values of parameters are those found in Huang et al. (2015). Parameter Symbol Value Unit Density ρ 2100 kg m^{-3} Poisson's ratio ν 0.3 - Elastic modulus E 70 MPa Cohesion c 10 kPa Internal friction angle ϕ 20° Dilation angle ψ 0° -

The geometry of the problem is depicted in Fig. 14, the soil material is discretized by 110×35 elements with $n_{pe} = 3^2$, resulting in $n_p = 21'840$ material points; a mesh spacing $h = 1 \text{ m}$ and rollers are imposed at the left and right domain limits while a no-slip condition is enforced at the base of the material. The parameters used for the solution are shown in Table ??.-

MPM solution to the elasto-plastic slump. The red lines indicate the solution obtained by Huang et al. (2015) and the coloured points indicate the second plastic strain invariant obtained with our CPDI2q solver. An intense shear zone progressively develops backwards from the toe of the slope, resulting in a circular failure mode.

The numerical solution to the elasto-plastic problem is shown in Fig. 15. An intense shear zone, highlighted by the second invariant of the plastic strain ϵ_{II} , develops at the toe of the slope as soon as the material yields and it propagates backwards to the top of the material. It results in a rotational slump. The geometry and the failure surface reported by Huang et al. (2015) are highlighted by the continuous and the dotted lines respectively.-

The maximal horizontal extent of the slump is smaller for the MPM solver with an M-C model, but the failure surface is in good agreement with the solution reported by Huang et al. (2015). They did not mention any use of a local damping in their implementation, and this can certainly explain the difference in the maximal extent. The local damping forces implemented in our solver should result in a smaller horizontal extent (because of the extra dissipation term introduced) but these should

635 not affect the geometry of the shear band. Despite the horizontal extent, our results appear coherent with those reported by Huang et al. (2015).-

5 Discussion

In this contribution, ~~an efficient~~ a fast and efficient explicit MPM solver is proposed that considers two variants (e.g., the cpGIMP-uGIMPM/cpGIMPM and the CPDI/CPDI2q ~~variant~~ under either an explicit or implicit

640 ~~The efficiency derives from the combined use of the connectivity array p2N with the built-in function accumarray(~~
~~+) to i) accumulate material point contributions to their associated nodes or ii) interpolate the updated nodal solutions to the~~
~~associated material points in a vectorized manner. The efficiency is demonstrated by the speed-up values obtained for the~~
~~evaluation of functions p2nsolve.m and mapN2p.m, which are 24 and 22 times faster, respectively, than an iterative~~
~~approach that would require multiple nested for-loops. For the cantilever beam, the MATLAB-based solver is, ad minima,~~
645 ~~twice faster than a Julia implementation~~ variants).

Regarding the ~~elastic compaction of a one element wide~~ compression of the elastic column, we report a good agreement of the numerical solver with previous explicit MPM implementations, such as Bardenhagen and Kober (2004). The same flaw of an explicit scheme is also experienced by the solver, i.e., a saturation of the error due to the specific ~~used~~ usage of an explicit scheme that resolves the wave propagation, thus preventing any static equilibrium to be reached. This confirms that our
650 ~~implementation is consistent with previous MPM implementations, especially for the implicit formulation where a quadratic~~
~~convergence is resolved.~~ However, the implicit implementation suffers from a decrease of the convergence rate for a fine mesh
resolution. Further work would be needed to investigate this decrease of convergence rate. This case also demonstrated that
cpGIMPM and CPDI variants have a similar computational cost and, this confirms the suitability of cpGIMPM with respect to
CPDI, as previously mentioned by Coombs et al. (2020); Charlton et al. (2017).

655 ~~Regarding~~ For the cantilever beam ~~problem~~, we report a good agreement of ~~our~~ the solver with the results ~~obtained by~~
~~Sadeghirad et al. (2011).~~ Furthermore of Sadeghirad et al. (2011), i.e., we report the vertical deflection of the beam to be very
close in both magnitude and timing (for the CPDI2-CPDI variant) to the FEM solution. ~~The beam almost recovered all the~~
~~vertical deflection it experienced during the gravitational loading.~~

~~Since we compared~~ However, we also report a slower execution time for the CPDI variant when compared to both cpGIMPM
660 ~~and CPDI2 implementations for the cantilever beam problem, we observed a difference regarding the computational efficiency;~~
~~the cpGIMP (e.g., it/s = 252.40) implementation is 3.5 times faster than the CPDI2 (e.g., it/s = 75.78) implementation for this~~
~~case. This is mainly due to the extra cost of calculation of the basis functions and their derivatives. Additional computational~~
~~resources are required to calculate these quantities, i.e., the basis function and their derivatives weights.~~ CPDI2q variants.

The elasto-plastic slump also demonstrates the solver to be efficient in capturing complex dynamics in the field of geomechanics.
665 The CDPI solution showed that the algorithm proposed by Simpson (2017) to return stresses when the material yields is
well suited to the slumping dynamics. However and as mentioned by Simpson (2017), such return mapping is only valid
under the assumption of a non-associated plasticity with no volumetric plastic strain. This particular case of isochoric plastic

670 deformations rises the issue of volumetric locking. In the actual implementation, no regularization techniques are considered. As a result, the pressure field experience severe locking for isochoric plastic deformations. One way to overcome locking phenomenons would be to implement the regularization technique initially proposed by Coombs et al. (2018) for quasi-static sMPM and GIMPM implementations.

Regarding the elasto-plastic collapse demonstrates the abilities of the solver, considering both the number of iterations per seconds and its accuracy with respect to, the numerical results demonstrate the solver to be in agreement with both previous experimental and numerical results (Huang et al., 2015; Bui et al., 2008). This confirms the ability of the solver to address elasto-plastic problems. However, this case indicates that extreme deformations are fatal for both cpGIMP and CPDI2q unless a domain update based on the determinant of the deformation gradient is chosen for the cpGIMP variant. Nevertheless, a splitting algorithm was the choice of whether to update or not the material point domain remains critical. Such question remains open and would require a more thorough investigation of the suitability of each of these domain updating variants. Nevertheless, the uGIMPM variant is a good candidate since, i) it is able to reproduce the experimental results of Bui et al. (2008) and, ii) it ensures numerical stability. However, one has to keep in mind its limited range of suitability regarding the deformation modes involved. If a cpGIMPM is selected, the splitting algorithm proposed in Gracia et al. (2019); Homel et al. (2016), and it could be implemented to mitigate the material point domain stretch.

In addition, the computational efficiency reached by the solver is higher than expected and is even higher in the elastic case with respect to what was reported by Sinaie et al. (2017). This confirms the efficiency of MATLAB for solid mechanics problems, provided a reasonable amount of time is spent on the vectorization of amount of distortion experienced by the material point domains during deformation. We did not selected the domain updating method based on the corners of the domain as suggested in Coombs et al. (2020). This is because such domain updating method necessitates to calculate additional shape functions between the corners of the domain of the MPM algorithm material point with their associated nodes. This results in an additional computational cost. Nevertheless, such variant is of interest and should be addressed as well when the computational performances are not the main concern.

The elasto-plastic slump also demonstrates the solver to be efficient in capturing complex dynamics in the field of geomechanics. Moreover the CDPI2q solution showed that the algorithm proposed by Simpson (2017) returns stresses when the material yields and is well suited to the slumping mechanics computational performance comes from the combined use of the connectivity array p2N with the built-in function accumarray() to i) accumulate material point contributions to their associated nodes or, ii) to interpolate the updated nodal solutions to the associated material points. When a residual performance is resolved, an overall performance gain (e.g., the amount of it/s) of 28 is reported. As an example, the functions p2nsolve.m and mapN2p.m are 24 and 22 times faster than an iterative algorithm when the residual performance is achieved. The overall performance gain is in agreement to other vectorised FEM codes, i.e., O'Sullivan et al. (2019) reported an overall gain of 25.7 for a optimised continuous Galerkin finite element code.

700 However, as mentioned by Simpson (2017), such return mapping is valid only under the assumption of a non-associated plasticity with no volumetric plastic strain. An iterative implementation would require multiple nested for-loops and a larger number of operations on smaller matrices, which increase the number of BLAS calls, thus inducing significant BLAS overheads

and decreasing the overall performance of the solver. This is limited by a vectorised code structure. However and as showed by the matrix multiplication problem, the L2 cache reuse is the limiting factor and, it ultimately affects the peak performance of the solver due to these numerous RAM-to-cache communications for larger matrices. Such problem is serious and, its influence is demonstrated by the delayed response in terms of performance for the function `constitutive.m`. However, we also have to mention that the overall residual performance was resolved only for a limited total number of material points. The performance drop of the function `constitutive.m` has never been achieved. Consequently, we suspect an additional decrease of overall performances of the solver for larger problems.

Our numerical investigations revealed that a domain-based approach in MPM fails when extremely large plastic deformations are involved. The overall performance achieved by the solver is higher than expected and, is even higher with respect to what was reported by Sinaie et al. (2017). We demonstrate that MATLAB is even more efficient than Julia, i.e., the elasto-plastic collapse. This can be avoided when a domain update based on the determinant of the deformation gradient is chosen a minimum 2.86 performance gain achieved compared to a similar Julia CPDI2q implementation. This confirms the efficiency of MATLAB for solid mechanics problems, provided a reasonable amount of time is spent on the vectorisation of the algorithm.

We also-

6 Conclusions

We have demonstrated the capability of MATLAB as an efficient language in regard to a material point method (MPM) implementation in an explicit or implicit formulation when bottleneck operations (e.g., calculations of the shape function or material point contributions) are vectorized. The MATLAB performances surpass those reached by an properly vectorised. The computational performances of MATLAB are even higher than those previously reported for a similar CPDI2q implementation in Julia, provided that built-in functions such as `accumarray()` are used. However, the numerical efficiency naturally decreases with the level of complexity of the chosen MPM variant (sMPM, GIMPM or CPDI/CPDI2q).

The vectorization tasks vectorisation activities we performed provide a fast and efficient MATLAB-based solver; however, the algorithmic structure MPM solver. Such vectorised code could be transposed to a more efficient language, such as the C-CUDA language, that is known to efficiently take advantage of vectorized vectorised operations.

As a final word, a future implementation of a poro-elasto-plastic mechanical solver could be applied to complex geomechanical problems such as landslide dynamics while benefiting from a faster numerical implementation in C-CUDA, thus resolving high three-dimensional resolutions in an a decent and affordable amount a time.

Code availability. The fMPMM-solver developed in this study is licensed under the GPLv3 free software licence. The latest version of the code is available for download from Bitbucket at: <https://bitbucket.org/ewyser/fmpmm-solver/src/master/> (last access: October 6, 2020). The fMPMM-solver archive (v1.0 and v1.1) is available from a permanent DOI repository (Zenodo) at: <https://doi.org/10.5281/zenodo.4068585> (Wyser et al., 2020). The fMPMM-solver software includes the reproducible codes used for this study.

Appendix A: Acronyms

Table A1. Acronyms used throughout the manuscript

PIC	P article-in- C ell
FLIP	F Luid I mplicit P article
FEM	F inite E lement M ethod
sMPM	standard M aterial P oint M ethod
GIMPM	G eneralized M aterial P oint M ethod
uGIMPM	u ndeformed G eneralized M aterial P oint M ethod
cpGIMPM	cp ontiguous p article G eneralized M aterial P oint M ethod
CPDI	C onvected P article D omain I nterpolation
CPDI2q	C onvected P article D omain I nterpolation 2 nd order q uadrilateral

Table B1. Variables of the structure arrays for the mesh `meD` and the material point `mpD` used in Code Fragment 1 & 2 shown in Figs. 4 & 5. `nDF` stores the local and global number of degrees of freedom, i.e., `nDF=[nNe, nN+DoF]`. The constant `nstr` is the number of stress components, according to the standard definition of the Cauchy stress tensor using the Voigt notation, e.g., $\sigma_p = (\sigma_{xx}, \sigma_{yy}, \sigma_{xy})$.

Variable	Description	Dimension
meD.	<code>nNe</code> nodes per element	<code>(1)</code>
	<code>nN</code> number of nodes	<code>(1)</code>
	<code>DoF</code> degree of freedom	<code>(1)</code>
	<code>nDF</code> number of DoF	<code>(1, 2)</code>
	<code>h</code> mesh spacing	<code>(1, DoF)</code>
	<code>x</code> node coordinates	<code>(nN, 1)</code>
	<code>y</code> node coordinates	<code>(nN, 1)</code>
	<code>m</code> nodal mass	<code>(nN, 1)</code>
	<code>p</code> nodal momentum	<code>(nDF(2), 1)</code>
	<code>f</code> nodal force	<code>(nDF(2), 1)</code>
mpD.	<code>n</code> number of points	<code>(1)</code>
	<code>l</code> domain half-length	<code>(np, DoF)</code>
	<code>V</code> volume	<code>(np, 1)</code>
	<code>m</code> mass	<code>(np, 1)</code>
	<code>x</code> point coordinates	<code>(np, DoF)</code>
	<code>p</code> momentum	<code>(np, DoF)</code>
	<code>s</code> stress	<code>(np, nstr)</code>
	<code>S</code> basis function	<code>(np, nNe)</code>
	<code>dSx</code> derivative in x	<code>(np, nNe)</code>
	<code>dSy</code> derivative in y	<code>(np, nNe)</code>
	<code>B</code> B matrix	<code>(nstr, nDF(1), np)</code>

Author contributions. EW wrote the original manuscript and developed, together with YP, the first version the solver (fMPMM-solver, v1.0). YA provided technical supports, assisted EW in the revision of the latest version of the solver (v1.1) and corrected specific parts of the solver. EW and YA wrote together the revised version of the manuscript. MJ and YP supervised the early stages of the study and provided guidance. All authors have reviewed and approved the final version of the paper.

740 *Competing interests.* The authors declare that they have no conflicts of interest.

Acknowledgements. [Yury Alkhimenkov gratefully acknowledges the support from the Swiss National Science Foundation \(grant no. 172691\).](#)
[Yury Alkhimenkov and Yury Y. Podladchikov gratefully acknowledge support from the Russian Ministry of Science and Higher Education \(project No. 075-15-2019-1890\).](#) The authors gratefully thank Johan Gaume for his comments that contributed to improve the overall quality of the manuscript.

745 References

- Abe, K., Soga, K., and Bandara, S.: Material point method for coupled hydromechanical problems, *Journal of Geotechnical and Geoenvironmental Engineering*, 140, 04013 033, 2014.
- Acosta, J. L. G., Vardon, P. J., Remmerswaal, G., and Hicks, M. A.: An investigation of stress inaccuracies and proposed solution in the material point method, *Computational Mechanics*, 65, 555–581, 2020.
- 750 Anderson Jr, C. E.: An overview of the theory of hydrocodes, *International journal of impact engineering*, 5, 33–59, 1987.
- Bandara, S. and Soga, K.: Coupling of soil deformation and pore fluid flow using material point method, *Computers and geotechnics*, 63, 199–214, 2015.
- Bandara, S., Ferrari, A., and Laloui, L.: Modelling landslides in unsaturated slopes subjected to rainfall infiltration using material point method, *International Journal for Numerical and Analytical Methods in Geomechanics*, 40, 1358–1380, 2016.
- 755 Bardenhagen, S., Brackbill, J., and Sulsky, D.: The material-point method for granular materials, *Computer methods in applied mechanics and engineering*, 187, 529–541, 2000.
- Bardenhagen, S. G. and Kober, E. M.: The generalized interpolation material point method, *Computer Modeling in Engineering and Sciences*, 5, 477–496, 2004.
- Baumgarten, A. S. and Kamrin, K.: A general fluid–sediment mixture model and constitutive theory validated in many flow regimes, *Journal*
- 760 *of Fluid Mechanics*, 861, 721–764, 2019.
- Beuth, L., Benz, T., Vermeer, P. A., and Więckowski, Z.: Large deformation analysis using a quasi-static material point method, *Journal of Theoretical and Applied Mechanics*, 38, 45–60, 2008.
- Bird, R. E., Coombs, W. M., and Giani, S.: Fast native-MATLAB stiffness assembly for SIPG linear elasticity, *Computers & Mathematics with Applications*, 74, 3209–3230, 2017.
- 765 Bui, H. H., Fukagawa, R., Sako, K., and Ohno, S.: Lagrangian meshfree particles method (SPH) for large deformation and failure flows of geomaterial using elastic–plastic soil constitutive model, *International journal for numerical and analytical methods in geomechanics*, 32, 1537–1570, 2008.
- Charlton, T., Coombs, W., and Augarde, C.: iGIMP: An implicit generalised interpolation material point method for large deformations, *Computers & Structures*, 190, 108–125, 2017.
- 770 Coombs, W. M. and Augarde, C. E.: AMPLE: A Material Point Learning Environment, *Advances in Engineering Software*, 139, 102 748, 2020.
- Coombs, W. M., Charlton, T. J., Cortis, M., and Augarde, C. E.: Overcoming volumetric locking in material point methods, *Computer Methods in Applied Mechanics and Engineering*, 333, 1–21, 2018.
- Coombs, W. M., Augarde, C. E., Brennan, A. J., Brown, M. J., Charlton, T. J., Knappett, J. A., Motlagh, Y. G., and Wang, L.: On Lagrangian
- 775 mechanics and the implicit material point method for large deformation elasto-plasticity, *Computer Methods in Applied Mechanics and Engineering*, 358, 112 622, 2020.
- Cortis, M., Coombs, W., Augarde, C., Brown, M., Brennan, A., and Robinson, S.: Imposition of essential boundary conditions in the material point method, *International Journal for Numerical Methods in Engineering*, 113, 130–152, 2018.
- Dabrowski, M., Krotkiewski, M., and Schmid, D.: MILAMIN: MATLAB-based finite element method solver for large problems, *Geochemistry, Geophysics, Geosystems*, 9, 2008.
- 780 Davis, T. A.: Suite Sparse, <https://people.engr.tamu.edu/davis/research.html>, 2013.

- de Koster, P., Tielen, R., Wobbes, E., and Möller, M.: Extension of B-spline Material Point Method for unstructured triangular grids using Powell–Sabin splines, *Computational Particle Mechanics*, pp. 1–16, 2020.
- de Souza Neto, E. A., Peric, D., and Owen, D. R.: *Computational methods for plasticity: theory and applications*, John Wiley & Sons, 2011.
- 785 de Vaucorbeil, A., Nguyen, V., and Hutchinson, C.: A Total-Lagrangian Material Point Method for solid mechanics problems involving large deformations, 2020.
- Dunatunga, S. and Kamrin, K.: Continuum modelling and simulation of granular flows through their many phases, *Journal of Fluid Mechanics*, 779, 483–513, 2015.
- Dunatunga, S. and Kamrin, K.: Continuum modeling of projectile impact and penetration in dry granular media, *Journal of the Mechanics*
790 *and Physics of Solids*, 100, 45–60, 2017.
- Fern, J., Rohe, A., Soga, K., and Alonso, E.: *The material point method for geotechnical engineering: a practical guide*, CRC Press, 2019.
- Gan, Y., Sun, Z., Chen, Z., Zhang, X., and Liu, Y.: Enhancement of the material point method using B-spline basis functions, *International Journal for numerical methods in engineering*, 113, 411–431, 2018.
- Gaume, J., Gast, T., Teran, J., van Herwijnen, A., and Jiang, C.: Dynamic anticrack propagation in snow, *Nature communications*, 9, 1–10,
795 2018.
- Gaume, J., van Herwijnen, A., Gast, T., Teran, J., and Jiang, C.: Investigating the release and flow of snow avalanches at the slope-scale using a unified model based on the material point method, *Cold Regions Science and Technology*, 168, 102 847, 2019.
- Gracia, F., Villard, P., and Richefeu, V.: Comparison of two numerical approaches (DEM and MPM) applied to unsteady flow, *Computational Particle Mechanics*, 6, 591–609, 2019.
- 800 Guilkey, J. E. and Weiss, J. A.: Implicit time integration for the material point method: Quantitative and algorithmic comparisons with the finite element method, *International Journal for Numerical Methods in Engineering*, 57, 1323–1338, 2003.
- Homel, M. A., Brannon, R. M., and Guilkey, J.: Controlling the onset of numerical fracture in parallelized implementations of the material point method (MPM) with convective particle domain interpolation (CPDI) domain scaling, *International Journal for Numerical Methods in Engineering*, 107, 31–48, 2016.
- 805 Huang, P., Li, S.-l., Guo, H., and Hao, Z.-m.: Large deformation failure analysis of the soil slope based on the material point method, *computational Geosciences*, 19, 951–963, 2015.
- Iaconeta, I., Larese, A., Rossi, R., and Guo, Z.: Comparison of a material point method and a galerkin meshfree method for the simulation of cohesive-frictional materials, *Materials*, 10, 1150, 2017.
- Leavy, R., Guilkey, J., Phung, B., Spear, A., and Brannon, R.: A convected-particle tetrahedron interpolation technique in the material-point
810 method for the mesoscale modeling of ceramics, *Computational Mechanics*, 64, 563–583, 2019.
- Moler, C.: MATLAB Incorporates LAPACK, <https://ch.mathworks.com/de/company/newsletters/articles/matlab-incorporates-lapack.html?refresh=true>, 2000.
- Nairn, J. A.: Material point method calculations with explicit cracks, *Computer Modeling in Engineering and Sciences*, 4, 649–664, 2003.
- Ni, R. and Zhang, X.: A precise critical time step formula for the explicit material point method, *International Journal for Numerical Methods*
815 *in Engineering*, 121, 4989–5016, 2020.
- O’Sullivan, S., Bird, R. E., Coombs, W. M., and Giani, S.: Rapid non-linear finite element analysis of continuous and discontinuous galerkin methods in matlab, *Computers & Mathematics with Applications*, 78, 3007–3026, 2019.

820 Sadeghirad, A., Brannon, R. M., and Burghardt, J.: A convected particle domain interpolation technique to extend applicability of the material point method for problems involving massive deformations, *International Journal for numerical methods in Engineering*, 86, 1435–1456, 2011.

Sadeghirad, A., Brannon, R., and Guilkey, J.: Second-order convected particle domain interpolation (CPDI2) with enrichment for weak discontinuities at material interfaces, *International Journal for numerical methods in Engineering*, 95, 928–952, 2013.

Simpson, G.: *Practical finite element modeling in earth science using matlab*, Wiley Online Library, 2017.

825 Sinaie, S., Nguyen, V. P., Nguyen, C. T., and Bordas, S.: Programming the material point method in Julia, *Advances in Engineering Software*, 105, 17–29, 2017.

Steffen, M., Kirby, R. M., and Berzins, M.: Analysis and reduction of quadrature errors in the material point method (MPM), *International journal for numerical methods in engineering*, 76, 922–948, 2008a.

Steffen, M., Wallstedt, P., Guilkey, J., Kirby, R., and Berzins, M.: Examination and analysis of implementation choices within the material point method (MPM), *Computer Modeling in Engineering and Sciences*, 31, 107–127, 2008b.

830 Stomakhin, A., Schroeder, C., Chai, L., Teran, J., and Selle, A.: A material point method for snow simulation, *ACM Transactions on Graphics (TOG)*, 32, 1–10, 2013.

Sulsky, D., Chen, Z., and Schreyer, H. L.: A particle method for history-dependent materials, *Computer methods in applied mechanics and engineering*, 118, 179–196, 1994.

835 Sulsky, D., Zhou, S.-J., and Schreyer, H. L.: Application of a particle-in-cell method to solid mechanics, *Computer physics communications*, 87, 236–252, 1995.

Vardon, P. J., Wang, B., and Hicks, M. A.: Slope failure simulations with MPM, *Journal of Hydrodynamics*, 29, 445–451, 2017.

Vermeer, P. A. and De Borst, R.: Non-associated plasticity for soils, concrete and rock, *HERON*, 29 (3), 1984, 1984.

Wallstedt, P. C. and Guilkey, J.: An evaluation of explicit time integration schemes for use with the generalized interpolation material point method, *Journal of Computational Physics*, 227, 9628–9642, 2008.

840 Wang, B., Hicks, M., and Vardon, P.: Slope failure analysis using the random material point method, *Géotechnique Letters*, 6, 113–118, 2016a.

Wang, B., Vardon, P., and Hicks, M.: Investigation of retrogressive and progressive slope failure mechanisms using the material point method, *Computers and Geotechnics*, 78, 88–98, 2016b.

845 Wang, B., Vardon, P. J., Hicks, M. A., and Chen, Z.: Development of an implicit material point method for geotechnical applications, *Computers and Geotechnics*, 71, 159–167, 2016c.

Wang, L., Coombs, W. M., Augarde, C. E., Cortis, M., Charlton, T., Brown, M., Knappett, J., Brennan, A., Davidson, C., Richards, D., et al.: On the use of domain-based material point methods for problems involving large distortion, *Computer Methods in Applied Mechanics and Engineering*, 355, 1003–1025, 2019.

850 Więckowski, Z.: The material point method in large strain engineering problems, *Computer methods in applied mechanics and engineering*, 193, 4417–4438, 2004.

Wyser, E., Alkhimenkov, Y., Jayboyedoff, M., and Podladchikov, Y.: fMPMM-solver, <https://doi.org/10.5281/zenodo.4068585>, <https://doi.org/10.5281/zenodo.4068585>, 2020.

York, A. R., Sulsky, D., and Schreyer, H. L.: The material point method for simulation of thin membranes, *International journal for numerical methods in engineering*, 44, 1429–1456, 1999.

855 Zhang, X., Chen, Z., and Liu, Y.: The material point method: a continuum-based particle method for extreme loading cases, Academic Press, 2016.